ANGEWANDTE MATHEMATIK

UND

INFORMATIK

Inflow-Implicit/Outflow-Explicit Finite Volume Methods for Solving Advection Equations

Karol Mikula, Mario Ohlberger, and Jozef Urbán

01/12 - N

UNIVERSITÄT MÜNSTER

INFLOW-IMPLICIT/OUTFLOW-EXPLICIT FINITE VOLUME METHODS FOR SOLVING ADVECTION EQUATIONS

KAROL MIKULA *, MARIO OHLBERGER †, AND JOZEF URBÁN ‡

Abstract. We introduce a new class of methods for solving non-stationary advection equations. The new methods are based on finite volume space discretizations and a semi-implicit discretization in time. Its basic idea is that outflow from a cell is treated explicitly while inflow is treated implicitly. This is natural, since we know what is outflowing from a cell at the old time step but we leave the method to resolve a system of equations determined by the inflows to a cell to obtain the solution values at the new time step. The matrix of the system in our inflow-implicit/outflow-explicit (I^2OE) method is determined by the inflow fluxes which results in a M-matrix yielding favourable stability properties for the scheme. Since the explicit (outflow) part is not always dominated by the implicit (inflow) part and thus some oscillations can occur, we build a stabilization based on the upstream weighted averages with coefficients determined by the flux-corrected transport approach [2, 19] yielding high resolution versions, S^1I^2OE and S^2I^2OE, of the basic scheme. We prove that our new method is exact for any choice of a discrete time step on uniform rectangular grids in the case of constant velocity transport of quadratic functions in any dimension. We also show its formal second order accuracy in space and time for 1D advection problems with variable velocity. Although designed for non-divergence free velocity fields, we show that the basic I^2OE scheme is locally mass conservative in case of divergence free velocity. Finally, we show L^2-stability for divergence free velocity in 1D on periodic domains independent of the choice of the time step, and L^∞-stability for the stabilized high resolution variants of the scheme. Numerical comparisons with the purely explicit schemes like the fully explicit up-wind and the Lax-Wendroff schemes were discussed in [13] and [14] where the basic I^2OE was originally introduced. There it has been shown that the new scheme has good properties with respect to a balance of precision and CPU time related to a possible choice of larger time steps in our scheme. In this contribution we compare the new scheme and its stabilized variants with other widely used implicit schemes, like the fully implicit up-wind and higher-order Gear's up-wind methods. Also in this comparison our new schemes show best behaviour with respect to stability and precision of computations for time steps several times exceeding the CFL stability condition. Our new stabilized methods are L^∞ stable, second order accurate for any smooth solution and with accuracy of order 2/3 for solutions with moving discontinuities. This is opposite to implicit up-wind schemes which have accuracy order 1/2 only. All these properties hold for any choice of time step thus making our new method attractive for practical applications.

Key words. advection equations, variable velocity, nonlinear conservation laws, level-set method, finite volume method, semi-implicit scheme.

AMS subject classifications. 35K20, 35L04, 35L60, 76M12, 76R50, 65M08.

1. Introduction. In this article we present the inflow-implicit/outflow-explicit (I^2OE) method, and its stabilized (S^1I^2OE, S^2I^2OE) high-resolution variants, for solving general time dependent variable velocity advection equations of the form

$$u_t + \mathbf{v} \cdot \nabla u = 0 \tag{1.1}$$

where $u \in \mathbb{R}^d \times [0, T]$ is the unknown function and $\mathbf{v}$ is a vector field which may vary in space, e.g. $\mathbf{v} = \mathbf{v}(x, u, \nabla u)$. Variable velocity vector fields arise in many applications, e.g. in transport equations with non-divergence free velocities or nonlinear conservation laws [11], in the Eulerian level set methods for evolving fronts [18], in a tangentially stabilized Lagrangean methods for evolving interfaces [16, 1] or in other

* Department of Mathematics, Slovak University of Technology, Radlinského 11, 81368 Bratislava, Slovakia (karol.mikula@stuba.sk).

† Institut für Numerische und Angewandte Mathematik, Universität Münster, Einsteinstr. 62, D-48149 Münster, Germany (mario.ohlberger@uni-muenster.de).

‡ Department of Mathematics, Slovak University of Technology, Radlinského 11, 81368 Bratislava, Slovakia and TatraMed spol. s r.o., Bratislava, Slovakia. (jozo.urban@gmail.com).

applications like an image segmentation by active contours in a form of generalized subjective surface method [4, 9, 17, 15, 20, 3]. In such case of image segmentation, the spatially varying vector field $\mathbf{v}(x)$ depends on the gradient of the image intensity function. For motion of level sets in normal direction with speed $F(x)$ we have $\mathbf{v} = F(x)\frac{\nabla u}{|\nabla u|}$ [18, 12]. In this case the basic I^2OE method coincides with the semi-implicit forward-backward diffusion approach recently presented by the authors in [12]. In the context of level set equations the originality of the approach in [12] consists in rewriting the level set equation for motion in normal direction in terms of an equation containing the forward and backward diffusion. Then naturaly, the forward diffusion dominated parts of the model are treated implicitly, while the backward diffusion dominated parts are treated explicitly. The resulting scheme is a semi-implicit second order numerical scheme that allows large time steps. Hence, our new I^2OE method presented in [13, 14] and in this paper can be seen as a generalization of the approach from [12] to arbitrary variable velocity advection equations.

The basic idea of our new I^2OE method is that outflow from a cell is treated explicitly while inflow is treated implicitly. Such an approach is natural, since we know what is flowing out from a cell at an old time step $n-1$ but we leave the method to resolve a system of equations determined by the inflows to obtain a new value in the cell at time step n. Since the matrix of the system is determined by the inflow fluxes, it is a M-matrix and thus it has favourable solvability and stability properties. It is worth to note that a similar idea to construct the M-matrix in the implicit part has also been introduced by Kuzmin and his co-authors by using a purely algebraic approach in the context of solving advection equations by the Galerkin finite element method combined usually with the Crank-Nicolson time stepping, see [10] for the latest state-of-the-art and related references.

Since the explicit (outflow) part is not always dominated by the implicit (inflow) part, some oscillations can occur in the basic I^2OE scheme. One way is to leave them propagate and perform some postprocessing of the numerical solution, or another way is to incorporate a stabilization mechanism into the scheme itself. As it was shown in [12], a special local averaging was sufficient to stabilize the forward-backward diffusion approach in order to get stable second order solution in case of smooth level set interface motion in normal direction, but in general, such local averaging does not guarrantee fulfilling sharply the discrete minimum-maximum principle. In this paper we build a new stabilization of the basic I^2OE scheme based on the so-called flux-corrected transport approach [2, 19] yielding L^∞ stable high resolution variants of the scheme.

We also present theoretical results for our new scheme, namely, its exactness for any choice of time step on uniform rectangular grids in the case of constant velocity transport of quadratic functions in any dimension and its formal second order accuracy in space and time for 1D advection problems with variable velocity. Although designed for non-divergence free velocity fields, we show that the basic I^2OE scheme is locally mass conservative in case of divergence free velocity. Finally, we show L^2-stability for divergence free velocity in 1D on periodic domains independent of the choice of the time step, and L^∞-stability for the stabilized high resolution variants of the scheme.

Numerical comparisons with the fully explicit schemes like the fully explicit upwind and the (limited) Lax-Wendroff method were discussed in [13] and [14]. There, the positive properties of the new scheme have been shown with respect to a balance of precision and CPU time. Thus, in this paper we concentrate mainly on a comparison of the new I^2OE scheme and its stabilized variants with the well-known and widely used implicit methods for solving advection equations. We show superior behaviour of our new schemes with respect to stability and precision of computations for time steps largely exceeding CFL stability condition in comparison with the fully implicit up-wind and higher-order Gear's up-wind methods. Our new schemes are L^∞ stable, second order accurate for smooth solutions and with accuracy of order $2/3$ for solutions with moving discontinuities, opposite to the implicit up-wind schemes which have accuracy order only $1/2$ in the discontinuous case. Moreover, all these properties hold for any choice of time step and thus make our new methods attractive from the point of view of practical applications where no concern on CFL restrictions is preferable.

The rest of the article is organized as follows. In Section 2 we introduce the general formulation of the basic and stabilized I^2OE schemes on unstructured grids in several space dimensions. In Section 3, for clarity and also due to the reasons of our theoretical study, we write a 1D version of the I^2OE scheme and also its higher dimensional form in the case of advective motion of level sets in normal direction in order to clearly see its relation to the forward-backward diffusion approach from [12]. In Section 4 we present theoretical results for our new schemes and in Section 5 we present several representative 1D and higher dimensional numerical experiments demonstrating interesting properties of the method.

2. The inflow-implicit/outflow-explicit scheme. Let us consider equation (1.1) in a bounded polygonal domain $\Omega \subset \mathbb{R}^d$, $d = 2, 3$, and time interval $[0, T]$. Let $\mathcal{Q}_h$ denote a primal polygonal partition of Ω. Let p be a finite volume (cell) of a corresponding dual Voronoi tessellation $\mathcal{T}_h$ with measure m_p and let e_{pq} be an edge between p and q, $q \in N(p)$, where $N(p)$ is a set of neighbouring finite volumes (i.e. $\bar{p} \cap \bar{q}$ has nonzero $(d-1)$-dimensional measure). Let us note that the Voronoi property is introduced just due to a formulation of the scheme for advective motion of level sets in normal direction, presented in Section 3.2, where approximation of the solution gradient is necessary. Let c_{pq} be the length of e_{pq} and n_{pq} be the unit outer normal vector to e_{pq} with respect to p. We shall consider $\mathcal{T}_h$ to be an admissible mesh in the sense of [5], i.e., there exists a representative point x_p in the interior of every finite volume p such that the joining line between x_p and x_q, $q \in N(p)$, is orthogonal to e_{pq}. We denote by x_{pq} the intersection of this line segment with the edge e_{pq}. The length of this line segment is denoted by d_{pq}, i.e. $d_{pq} := |x_q - x_p|$. As we have build $\mathcal{T}_h$ based on the primal mesh $\mathcal{Q}_h$, we assume that the points x_p coincide with the vertices of $\mathcal{Q}_h$. Let us denote by u_p a (constant) value of the solution in a finite volume p computed by the scheme. For the solution representation inside the finite volume p we either use this value u_p or a reconstructed (but again constant) value denoted by $\overline{u}_p$. A constant value of the solution assigned to the edge e_{pq} (given again by a reconstruction) is denoted by $\overline{u}_{pq}$.

In order to motivate our new scheme, let us rewrite (1.1) in the formally equivalent form with conserving and non-conserving parts [7, 8]

$$u_t + \nabla \cdot (\mathbf{v}u) - u\nabla \cdot \mathbf{v} = 0. \tag{2.1}$$

Integrating (2.1) over a finite volume p then yields

$$\int_p u_t \; dx + \int_p \nabla \cdot (\mathbf{v}u) \; dx - \int_p u\nabla \cdot \mathbf{v} \; dx = 0.$$

Using a constant representation of the solution on the cell p denoted by $\overline{u}_p$ and applying the divergence theorem we get

$$\int_p u_t \; dx + \sum_{q \in N(p)} \int_{e_{pq}} u\mathbf{v} \cdot n_{pq} \; ds - \overline{u}_p \sum_{q \in N(p)} \int_{e_{pq}} \mathbf{v} \cdot n_{pq} \; ds = 0.$$

Denoting by $\overline{u}_{pq}$ another representative constant value of the solution on the interface e_{pq}, we further get

$$\int_p u_t \; dx + \sum_{q \in N(p)} \overline{u}_{pq} \int_{e_{pq}} \mathbf{v} \cdot n_{pq} \; ds - \overline{u}_p \sum_{q \in N(p)} \int_{e_{pq}} \mathbf{v} \cdot n_{pq} \; ds = 0.$$

If we denote the integrated fluxes in the inward normal direction to the finite volume p by

$$\bar{v}_{pq} = - \int_{e_{pq}} \mathbf{v} \cdot n_{pq} \; ds, \tag{2.2}$$

we finally arrive at the balance law

$$\int_p u_t \; dx + \sum_{q \in N(p)} \bar{v}_{pq}(\overline{u}_p - \overline{u}_{pq}) = 0. \tag{2.3}$$

The major new idea of our scheme is to split the resulting fluxes into the corresponding inflow and outflow parts to the cell p. This is done by defining

$$a_{pq}^{in} = \max(\bar{v}_{pq}, 0), \quad a_{pq}^{out} = \min(\bar{v}_{pq}, 0). \tag{2.4}$$

We then approximate u_t by the time difference $\frac{u_p^n - u_p^{n-1}}{\tau}$, where τ is a uniform time step size, and take the inflow parts implicitly and the outflow parts explicitly in (2.3). This yields the following system of equations for the finite volume solution $u_p^n, p \in \mathcal{T}_h$ at the n-th discrete time step

$$u_p^n + \frac{\tau}{m_p} \sum_{q \in N(p)} a_{pq}^{in}(\overline{u}_p^n - \overline{u}_{pq}^n) = u_p^{n-1} - \frac{\tau}{m_p} \sum_{q \in N(p)} a_{pq}^{out}(\overline{u}_p^{n-1} - \overline{u}_{pq}^{n-1}) \tag{2.5}$$

for all $p \in \mathcal{T}_h$.

The most natural choice for reconstructions $\overline{u}_p^m$ and $\overline{u}_{pq}^m$, $m = n, n-1$ is given by

$$\overline{u}_p^m = u_p^m, \;\; \overline{u}_{pq}^m = \frac{1}{2}(u_p^m + u_q^m) \tag{2.6}$$

and leads to the basic **I^{2}OE scheme**

$$u_p^n + \frac{\tau}{2m_p} \sum_{q \in N(p)} a_{pq}^{in}(u_p^n - u_q^n) = u_p^{n-1} - \frac{\tau}{2m_p} \sum_{q \in N(p)} a_{pq}^{out}(u_p^{n-1} - u_q^{n-1}) \tag{2.7}$$

which for a uniform squared grids in two space dimensions with a finite volume side width h reduces to the following simple system

$$u_p^n + \frac{\tau}{2h^2} \sum_{q \in N(p)} a_{pq}^{in}(u_p^n - u_q^n) = u_p^{n-1} - \frac{\tau}{2h^2} \sum_{q \in N(p)} a_{pq}^{out}(u_p^{n-1} - u_q^{n-1}). \tag{2.8}$$

Before proceeding further let us remark that, the equation (2.3) has the form of a discretization of a diffusion equation, where $\bar{v}_{pq}$ would represent the so-called transmissive coefficients (integrated diffusion fluxes divided by distances between cell centers). In a standard forward diffusion all these coefficients are strictly positive which leads to a weigted averaging of the solution and the implicit schemes are natural in this case. On the other hand the negative coefficients would correspond to a backward diffusion in which case information propagates outside the cell and explicit schemes are thus natural. In our case the sign of the coefficients is given by the inflow or outflow character of the cell boundary and the inflow-implicit/outflow-explicit approach is thus natural. This forward-backward diffusion relationship with the inflow-outflow fluxes is inspired by [12] where the forward-backward diffusion formulation was used for solving advective motion of level sets in normal direction. Let us also note that a term h^{d-1} is included in the definition of the numerical fluxes $\bar{v}_{pq}$ and a term h^d in definition of m_p. Thus, taking this into account we see that a τ/h term is in front of the sums in (2.8) which is standard in advection discretization schemes. It is also well-known that in any second order scheme for solving advection equations one can identify the "forward diffusion" part (like the first order up-winding) and the "backward diffusion" part (additional sharpening terms comming (sometimes surprisingly) from the second order Taylor's expansions), a classical example is e.g. the Lax-Wendroff scheme [11]. In our method this splitting arises naturally and, as we will see theoretically in Section 4, it gives the second order accuracy. Since the "backward diffusion" part of the scheme is clearly given, its stabilization can be built straightforwardly if it is necessary to supress some (not unboundedly growing) oscillations.

The basic scheme (2.7) allows to use any time step size τ and obtain a solution of the linear system given by the left hand implicit side. This follows from the M-matrix property of the system and we call it the *solvability property* of the scheme. However, the right hand explicit side may cause oscillations especially in case of singularities or large gradients in a solution. These oscillations do not grow unboundedly in time, but if one prefers to remove them we present here a strategy how to make our method *unconditionally stable* in the L^∞ sense and keep its *second order accuracy* for smooth solutions. The stabilization approach is based on an adaptive upstream weighted choice for the averages $\overline{u}^m_{pq}, m = n, n-1$ at the cell interfaces. Instead of taking $\overline{u}^m_{pq} = \frac{1}{2}(u^m_p + u^m_q)$ as suggested for the basic scheme, we relax (2.6) to the choice

$$\overline{u}^m_p = u^m_p, \;\; \overline{u}^m_{pq} = (1-\theta^m_{pq})u^m_p + \theta^m_{pq}u^m_q \tag{2.9}$$

for some weighting parameter $\theta^m_{pq} \in [0,1]$ that we will choose locally in such a way that the resulting scheme becomes unconditionally stable in L^∞. With this relaxation we recover the basic scheme for $\theta^n_{pq} = \theta^{n-1}_{pq} = 1/2$, while $\theta^m_{pq} = 1$ corresponds to full up-wind for inflows (and full down-wind for outflows) and $\theta^m_{pq} = 0$ to full down-wind for inflows (and full up-wind for outflows). Since in our scheme the inflows appear in the implicit part, i.e. with index $m = n$, and outflows appear in the explicit part, i.e. for $m = n-1$, we will use notation $\theta^{in,n}_{pq}$ for inflow relaxation parameters and $\theta^{out,n-1}_{pq}$ for outflow relaxation parameters. Plugging reconstructions (2.9) in both inflow-implicit and outflow-explicit parts of (2.5) we get

$$\begin{aligned} & u^n_p + \frac{\tau}{m_p}\sum_{q\in N(p)} a^{in}_{pq}\left(u^n_p - \left((1-\theta^{in,n}_{pq})u^n_p + \theta^{in,n}_{pq}u^n_q\right)\right) = \\ & u^{n-1}_p - \frac{\tau}{m_p}\sum_{q\in N(p)} a^{out}_{pq}\left(u^{n-1}_p - \left((1-\theta^{out,n-1}_{pq})u^{n-1}_p + \theta^{out,n-1}_{pq}u^{n-1}_q\right)\right) \end{aligned} \tag{2.10}$$

from where we obtain the general form of a **stabilized I^{2}OE scheme**

$$u_p^n + \frac{\tau}{m_p} \sum_{q \in N(p)} \theta_{pq}^{in,n} a_{pq}^{in} (u_p^n - u_q^n) = u_p^{n-1} - \frac{\tau}{m_p} \sum_{q \in N(p)} \theta_{pq}^{out,n-1} a_{pq}^{out} (u_p^{n-1} - u_q^{n-1}) \quad (2.11)$$

where $\theta_{pq}^{out,n-1}$, $\theta_{pq}^{in,n}$ will be chosen using ideas of the so-called flux-corrected transport (FCT) methodology [2, 19]. The stabilized I^{2}OE scheme can be understood as a high-resolution variant of the basic I^{2}OE scheme which may locally decrease the outflow contributions, and, when not considering the outflows at all, it corresponds to a fully implicit up-wind method, where only inflows are considered. The local choice of the relaxation parameters will be done in such a way, that the stabilized I^{2}OE scheme reduces to the basic I^{2}OE in case of well resolved smooth solutions (and thus it is second order in smooth case), whereas it switches locally towards a fully implicit discretization at grid points where the minimum-maximum principle would be violated. We show by numerical computations that unlike the classical first order implicit up-wind method which has for linearly advected solutions with discontinuities convergence order 1/2, the new method has in such cases convergence order 2/3 for any choice of time step.

As noticed above, the choice of θ-stabilization coefficients follows the FCT approach. In our semi-implicit method, the only part which may cause the violation of the global minimum-maximum principle is the right hand explicit side of 2.11. Thus, we require that the relaxation parameters $\theta_{pq}^{out,n-1}$ are chosen in such a way that the following two conditions are fulfilled locally in every finite volume p

$$u_p^{n-1} - \frac{\tau}{m_p} \sum_{q \in N(p)} \theta_{pq}^{out,n-1} a_{pq}^{out} (u_p^{n-1} - u_q^{n-1}) \leq u_p^{max,n-1}, \quad (2.12)$$

$$u_p^{n-1} - \frac{\tau}{m_p} \sum_{q \in N(p)} \theta_{pq}^{out,n-1} a_{pq}^{out} (u_p^{n-1} - u_q^{n-1}) \geq u_p^{min,n-1}. \quad (2.13)$$

Here, $u_p^{max,n-1}$ and $u_p^{min,n-1}$ denote a maximum, respectively minimum in a local neighbourhood of p at time step $n-1$. A particular choice of the parameters $\theta_{pq}^{out,n-1}$ is determined as follows. Let us denote by n^{out} the number of nonzero outflows from the finite volume p, i.e.

$$n^{out} = - \sum_{q \in N(p)} \text{sign}(a_{pq}^{out}).$$

For all $q \in N(p)$ where $a_{pq}^{out} < 0$ and $(u_p^{n-1} - u_q^{n-1}) \neq 0$ we require that the following two conditions are satisfied

$$\frac{1}{n^{out}} u_p^{n-1} - \frac{\tau}{m_p} \theta_{pq}^{out,n-1} a_{pq}^{out} (u_p^{n-1} - u_q^{n-1}) \leq \frac{1}{n^{out}} u_p^{max,n-1}, \quad (2.14)$$

$$\frac{1}{n^{out}} u_p^{n-1} - \frac{\tau}{m_p} \theta_{pq}^{out,n-1} a_{pq}^{out} (u_p^{n-1} - u_q^{n-1}) \geq \frac{1}{n^{out}} u_p^{min,n-1}. \quad (2.15)$$

It is clear that by summation of the conditions (2.14) over all $q \in N(p)$ we get (2.12) and similarly by summation of (2.15) we get (2.13). The conditions (2.14), (2.15) are not necessarily optimal ones, but they are sufficient to get (2.12) and (2.13). Since on the right hand side of (2.12), (2.13) there are local minima and maxima which are inside the range of the global minimum and maximum at the time step $n-1$, due to the M-matrix property of the system on the left hand side of (2.11), we have that the overall solution in the new time step fulfills the global minimum-maximum principle. From (2.14) and (2.15) we get two conditions for $\theta_{pq}^{out,n-1}$

$$\theta_{pq}^{out,n-1} \le \frac{\frac{1}{n^{out}}(u_p^{max,n-1} - u_p^{n-1})}{-\frac{\tau}{m_p} a_{pq}^{out}(u_p^{n-1} - u_q^{n-1})}, \quad \text{if } (u_p^{n-1} - u_q^{n-1}) > 0, \tag{2.16}$$

$$\theta_{pq}^{out,n-1} \le \frac{\frac{1}{n^{out}}(u_p^{min,n-1} - u_p^{n-1})}{-\frac{\tau}{m_p} a_{pq}^{out}(u_p^{n-1} - u_q^{n-1})}, \quad \text{if } (u_p^{n-1} - u_q^{n-1}) < 0 \tag{2.17}$$

from which we define

$$\theta_{pq}^{out,n-1} = \text{Min}\left(\frac{1}{2}, \frac{m_p(u_p^{max,n-1} - u_p^{n-1})}{\tau n^{out} a_{pq}^{out}(u_q^{n-1} - u_p^{n-1})}\right) \text{ if } a_{pq}^{out}(u_q^{n-1} - u_p^{n-1}) > 0 \tag{2.18}$$

$$\theta_{pq}^{out,n-1} = \text{Min}\left(\frac{1}{2}, \frac{m_p(u_p^{min,n-1} - u_p^{n-1})}{\tau n^{out} a_{pq}^{out}(u_q^{n-1} - u_p^{n-1})}\right) \text{ if } a_{pq}^{out}(u_q^{n-1} - u_p^{n-1}) < 0. \tag{2.19}$$

If $a_{pq}^{out} = 0$ or $u_p^{n-1} - u_q^{n-1} = 0$, $\theta_{pq}^{out,n-1}$ could be theoretically arbitrary, but we set

$$\theta_{pq}^{out,n-1} = \frac{1}{2}, \text{ if } a_{pq}^{out}(u_q^{n-1} - u_p^{n-1}) = 0. \tag{2.20}$$

Finally, it remains to define the relaxation parameters $\theta_{pq}^{in,n}$ for the implicit inflow parts. If $\theta_{pq}^{in,n}$ is considered for an inflow face to volume p, it is natural that $\theta_{qp}^{out,n-1}$ is associated with an outflow face of the neighboring cell q. Thus, a natural choice that makes the reconstruction $\overline{u}_{pq}^n$ at the interface e_{pq} unique, is

$$\theta_{pq}^{in,n} = 1 - \theta_{qp}^{out,n-1} \tag{2.21}$$

where $\theta_{qp}^{out,n-1}$ is defined through (2.18)-(2.20). The scheme (2.11) with the choice of relaxation parameters given by (2.18)-(2.21) represent our first stabilized $\mathbf{S^1I^2OE}$ scheme. Let us note that our definitions of relaxation parameters ensure that for outflow faces we always have $\theta_{pq}^{out,n-1} \in [0, 1/2]$ and for inflow faces $\theta_{pq}^{in,n} \in [1/2, 1]$. Thus, the relaxation may only shift the reconstruction at cell interfaces towards an upstream average. The conditions (2.18)-(2.20) guarantee L^∞ stability, while condition (2.21) keeps the scheme consistent and ensures uniqueness of the cell interface reconstructions.

Performing numerical experiments, we have found and built also a second approach to stabilization that results in our $\mathbf{S^2I^2OE}$ scheme which is given by a two-step procedure in every discrete time step:

1st step: first use the basic I^{2}OE scheme, i.e. solve (2.11) with $\theta_{pq}^{in,n} = \theta_{pq}^{out,n-1} = 1/2$.
2nd step: if $u_p^n > u_p^{max,n-1}$ or $u_p^n < u_p^{min,n-1}$, we redefine $\theta_{pq}^{out,n-1}$ and $\theta_{qp}^{in,n}$ according to (2.18)-(2.21). (2.22)

The usage of the S^{2}I^{2}OE scheme is motivated by the fact that conditions (2.12), (2.13) may be too strong. Although they are not fulfilled sharply, the implicit part can keep the numerical solution in the minimum-maximum range. Thus, we mark the points where the minimum-maximum principle is violated when applying the basic I^{2}OE scheme and only in those points we redefine the relaxation parameters. On the first view, this approach seems slower concerning CPU than S^{1}I^{2}OE, because we have to solve the linear system twice. But, on the other hand, the redifinition of relaxation parameters, which takes its own CPU time, occurs only in few points while in S^{1}I^{2}OE it is done in every grid point. Our computational experience is that S^{2}I^{2}OE scheme is only slightly (like 10-20 %) slower than S^{1}I^{2}OE scheme while, especially in case of smooth solutions, it increases precision significantly.

Further useful modification of both stabilized schemes is that we can consider $u_p^{max,n-1}$ and $u_p^{min,n-1}$ in (2.12), (2.13) and subsequent formulas taking into account a local quadratic reconstruction of the numerical solution at time step $n-1$. This can be useful, because the maximum (minimum) does not necessarily transfer to a grid point in a consecutive time step. The quadratic reconstruction allows the reconstructed numerical solution to be slightly higher (lower) than just values at grid points and thus keeps overall maximum (minimum) with higher order accuracy. In particular, it makes our stabilized S^{2}I^{2}OE method exact for an advection of a quadratic function by a constant velocity for any choice of time step, similarly to such property of the basic I^{2}OE scheme, because the θ coefficients are not redefined when using quadratic reconstruction.

We summarize our new inflow-implicit/outflow-explicit methods in the following general definition.

Definition 2.1 (I^{2}OE schemes) *Let initial data $u_0 \in C^0(\Omega)$ and Dirichlet boundary data $u_D \in C^0(\partial\Omega \times [0,T])$ be given. Furthermore, let R_p and R_{pq} denote suitable local reconstructions of the solution on the cell p and the interface e_{pq}, respectively and g_{pq} denote a suitable numerical flux that approximates $-\int_{e_{pq}} \mathbf{v} \cdot n_{pq}\, ds$. These operators may differ depending on the inflow or outflow character of the cell interface (such dependence will be denoted by superscripts in and out).*

Then the general inflow-implicit/ outflow-explicit method (I^{2}OE) is defined as follows:

Initial data: *For $n = 0$ define the piecewise constant approximation u_h^0 through*

$$u_h^0|_p(x) := u_p^0 := \pi_p(u_0), \qquad \forall x \in p, p \in \mathcal{T}_h, \tag{2.23}$$

where $\pi_p : C^0(p) \to \mathbb{P}_0(p)$ is a suitable local projection to a constant.

Time step $(\mathbf{n-1}) \to \mathbf{n}$: *For $n > 0$ we define u_h^n through $u_p^n, p \in \mathcal{T}_h$ as follows*

a) Definition of boundary values at time t^n: For all $x_p \in \partial\Omega$ we set

$$u_p^n := u_D(x_p, t^n). \tag{2.24}$$

b) Definition of the interior values at time t^n:

i) Inflow/outflow splitting of the fluxes. For all interfaces e_{pq} we define

$$a_{pq}^{in,n} = \max(g_{pq}^{in}(\mathbf{v}, u_h^n), 0), \quad a_{pq}^{out,n-1} = \min(g_{pq}^{out}(\mathbf{v}, u_h^{n-1}), 0). \tag{2.25}$$

ii) For all $x_p \in \Omega \setminus \partial\Omega$ we define u_p^n as the solution of the following linear system

$$u_p^n + \frac{\tau}{m_p} \sum_{q \in N(p)} a_{pq}^{in,n} (R_p^{in}(u_h^n) - R_{pq}^{in}(u_h^n))$$
$$= u_p^{n-1} + \frac{\tau}{m_p} \sum_{q \in N(p)x} a_{pq}^{out,n-1} (R_p^{out}(u_h^{n-1}) - R_{pq}^{out}(u_h^{n-1})). \quad (2.26)$$

Note that (2.25) and (2.26) may result in a non-linear system of equations for u_h^n, if the velocity field depends on the solution.

b) Definition of u_h^n:
We define the piecewise constant approximation u_h^n as

$$u_h^n|_p(x) := u_p^n, \qquad \forall x \in p, p \in \mathcal{T}_h.$$

A specific I^{2}OE scheme is obtained by specifying the reconstruction operators R_p^{in}, R_{pq}^{in}, R_p^{out}, R_{pq}^{out} and the numerical flux function g_{pq}^{in}, g_{pq}^{out}. The most natural choice of reconstruction operators are given in (2.6) and (2.2) and lead to our basic **I^{2}OE scheme**. More sophisticated choices are given by (2.9) with stabilization parameters chosen from (2.18)–(2.21), or from (2.22) and lead to the **S^{1}I^{2}OE**, and **S^{2}I^{2}OE** schemes, respectively. These schemes are used in all computations presented in Section 5. Further particular choices of reconstructions are possible, e.g. a local averaging, as presented in the context of motion of level sets in normal direction in [12].

3. Special cases of the I^{2}OE scheme.

For clearer exposition and to prepare for the theoretically analysis in Section 4, we now detail the method in two particular cases, for one dimensional transport with variable velocity, and for motion of level sets in normal direction.

3.1. I^{2}OE scheme for 1D variable velocity case.

Let us derive the scheme for the one-dimensional equation

$$u_t + v u_x = 0, \quad (3.1)$$

where $v = v(x)$. Again (3.1) is written in the form

$$u_t + (vu)_x - u v_x = 0, \quad (3.2)$$

and integrated in p_i, the cell with the spatial index i, length h, center point x_i, left border $x_{i-\frac{1}{2}}$ and right border $x_{i+\frac{1}{2}}$. Let us denote $v_i = v(x_i)$, $v_{i-\frac{1}{2}} = v(x_{i-\frac{1}{2}})$, $v_{i+\frac{1}{2}} = v(x_{i+\frac{1}{2}})$, u_i^n the value of the numerical solution at time step n and $\overline{u}_i^n, \overline{u}_{i-\frac{1}{2}}^n$ the reconstructed values. Using the Newton-Leibniz formula we get

$$\int_{p_i} u_t \; dx + v_{i+\frac{1}{2}} \overline{u}_{i+\frac{1}{2}} - v_{i-\frac{1}{2}} \overline{u}_{i-\frac{1}{2}} - \overline{u}_i (v_{i+\frac{1}{2}} - v_{i-\frac{1}{2}}) = 0,$$

which can be rewritten as

$$\int_{p_i} u_t \; dx + v_{i-\frac{1}{2}} (\overline{u}_i - \overline{u}_{i-\frac{1}{2}}) + (-v_{i+\frac{1}{2}})(\overline{u}_i - \overline{u}_{i+\frac{1}{2}}) = 0.$$

If $v_{i-\frac{1}{2}} > 0$ it represents inflow from the left to the cell and if $(-v_{i+\frac{1}{2}}) > 0$ it represents inflow from the right to the cell. If the signs are opposite it represents outflows. Thus, we define

$$a^{in}_{i-\frac{1}{2}} = \max(v_{i-\frac{1}{2}}, 0), \quad a^{out}_{i-\frac{1}{2}} = \min(v_{i-\frac{1}{2}}, 0),$$
$$a^{in}_{i+\frac{1}{2}} = \max(-v_{i+\frac{1}{2}}, 0), \quad a^{out}_{i+\frac{1}{2}} = \min(-v_{i+\frac{1}{2}}, 0).$$

If we use a finite difference approximation of the time derivative, take inflow implicitly and outflow explicitly and use the simple reconstructions $\overline{u}^n_i = u^n_i$, $\overline{u}^n_{i-\frac{1}{2}} = \frac{1}{2}(u^n_i + u^n_{i-1})$ in both time steps, we end up with the basic **one-dimensional I^{2}OE scheme**:

$$\begin{aligned} u^n_i + \frac{\tau}{2h} a^{in}_{i-\frac{1}{2}}(u^n_i - u^n_{i-1}) + \frac{\tau}{2h} a^{in}_{i+\frac{1}{2}}(u^n_i - u^n_{i+1}) = \\ u^{n-1}_i - \frac{\tau}{2h}\left(a^{out}_{i-\frac{1}{2}}(u^{n-1}_i - u^{n-1}_{i-1}) + a^{out}_{i+\frac{1}{2}}(u^{n-1}_i - u^{n-1}_{i+1})\right) . \end{aligned} \tag{3.3}$$

The scheme (3.3) requires to solve a tridiagonal system in every time step which is very fast using the standard tridiagonal solver (also called the Thomas algorithm). The stabilized one-dimensional **S^{1}I^{2}OE** and **S^{2}I^{2}OE** schemes are obtained by (2.11) with the formulas (2.18)-(2.21) and (2.18)-(2.22), respectively.

3.2. I^{2}OE scheme for motion of level sets in normal direction. In the case of motion of level sets in normal direction we consider equation (1.1) with velocity depending on the gradient of solution, i.e. $\mathbf{v} = F\frac{\nabla u}{|\nabla u|}$. Let us consider cartesian grids in two space dimensions with finite volume side width h and define

$$\overline{v}_{pq} = Fh\,\frac{(\overline{u}^{n-1}_p - \overline{u}^{n-1}_{pq})}{(h/2)|\nabla u^{n-1}_{pq}|} = \frac{2F(\overline{u}^{n-1}_p - \overline{u}^{n-1}_{pq})}{|\nabla u^{n-1}_{pq}|} \tag{3.4}$$

where $|\nabla u^{n-1}_{pq}|$ is computed by the diamond-cell strategy as detailed in [12]. Pluging expression (3.4) for integrated inward fluxes into the basic I^{2}OE scheme (2.8) and comparing it with the scheme (2.5) in [12] we see that they form exactly the same system. One can also see the correspondence of the forward diffusion coefficients in [12] and inflow coefficients in the I^{2}OE scheme (2.8), respectively the backward diffusion coefficients in [12] and outflow coefficients in the I^{2}OE scheme (2.8). The FBD and FBD2 schemes from [12] are obtained using their reconstruction stencils (Definitions 2.3 and 3.1), and the role of the forward diffusion contribution D^f_p respectively the backward diffusion contribution D^b_p in general Definition 2.1 of [12] is played by the total inflow D^{in}_p respectively the total outflow D^{out}_p defined by

$$D^{in}_p = \sum_{q\in N(p)} a^{in}_{pq}, \qquad D^{out}_p = \sum_{q\in N(p)} a^{out}_{pq} . \tag{3.5}$$

Numerical experiments for such an I^{2}OE scheme are presented in [12] and also the results of the new stabilized versions of the basic scheme presented in this paper in Section 5.3 are similar to those.

4. Analysis of the scheme. The aim of this section is to give some theoretical backup for the I^{2}OE schemes. In particular we address local mass conservation, exactness for transport of quadratic polynomials with constant velocity with arbitrary time steps, formal order of consistency, $L^\infty(L^2)$ stability, as well as $L^\infty(L^\infty)$ stability. As we first look at local mass conservation, let us first recall that such property is automatically satisfied for the general class of finite volume schemes in conservation form, defined as follows.

Definition 4.1 (Finite volume scheme in conservation form) *Let $\Theta \in [0,1]$. A finite volume scheme is in conservation form if it can be written in the form*

$$u_p^n - u_p^{n-1} = -\frac{\tau}{m_p}\Big(\Theta \sum_{q\in N(p)} g_{pq}^n + (1-\Theta)\sum_{q\in N(p)} g_{pq}^{n-1}\Big).$$

where the fluxes need to be conservative in the sense that $g_{pq} = -g_{qp}$. In 1D on uniform partitions this reduces to

$$u_i^n - u_i^{n-1} = -\frac{\tau}{h}\Big(\Theta(g_{i+1/2}^n - g_{i-1/2}^n) + (1-\Theta)(g_{i+1/2}^{n-1} - g_{i-1/2}^{n-1})\Big).$$

Lemma 4.2 (Local conservation property) *For divergence free velocity field, the basic* I^{2}OE *is locally mass conservative and can be written in conservation form with numerical fluxes at inflow boundaries (with respect to cell p) $g_{pq} := g_{pq}^{in} := \frac{1}{2}(g_{pq}^{in,n} + g_{pq}^{in,n-1})$ with $g_{pq}^{in,n} := -a_{pq}^{in}u_q^n, g_{pq}^{in,n-1} := -a_{pq}^{in}u_p^{n-1}$ and at outflow boundaries $g_{pq} := g_{pq}^{out} := \frac{1}{2}(g_{pq}^{out,n} + g_{pq}^{out,n-1})$ and $g_{pq}^{out,n} := -a_{pq}^{out}u_p^n, g_{pq}^{out,n-1} := -a_{pq}^{out}u_q^{n-1}$. The conservation property holds, as we have with these definitions*

$$g_{pq}^{in} = -g_{qp}^{out}, \quad \textit{or respectively} \quad g_{pq}^{out} = -g_{qp}^{in}.$$

In the simple 1D case with constant positive velocity, the basic I^{2}OE *scheme thus reads*

$$u_i^n - u_i^{n-1} = -\frac{\tau}{h}\Big(\underbrace{\frac{v}{2}(u_i^n + u_{i+1}^{n-1})}_{=:g_{i+1/2}} - \underbrace{\frac{v}{2}(u_{i-1}^n + u_i^{n-1}))}_{=:g_{i-1/2}}\Big).$$

It is locally conservative with $\Theta := \frac{1}{2}$ and the following definition of the fluxes

$$g_{i+1/2}^n := vu_i^n, g_{i+1/2}^{n-1} := vu_{i+1}^{n-1}, g_{i-1/2}^n := vu_{i-1}^n, g_{i-1/2}^{n-1} := vu_i^{n-1}.$$

Proof. The divergence free velocity field implies in our discrete setting that we have for a cell p

$$\sum_{q\in N(p)} a_{pq}^{in} + \sum_{q\in N(p)} a_{pq}^{out} = 0.$$

This implies a rewriting of the I^{2}OE scheme as follows

$$\begin{aligned}
u_p^n &= u_p^{n-1} - \frac{\tau}{2m_p}\sum_{q\in N(p)} a_{pq}^{in}(u_p^n - u_q^n) - \frac{\tau}{2m_p}\sum_{q\in N(p)} a_{pq}^{out}(u_p^{n-1} - u_q^{n-1})\\
&= u_p^{n-1} - \frac{\tau}{2m_p}\sum_{q\in N(p)} a_{pq}^{in}u_p^n + \frac{\tau}{2m_p}\sum_{q\in N(p)} a_{pq}^{in}u_q^n\\
&\quad -\frac{\tau}{2m_p}\sum_{q\in N(p)} a_{pq}^{out}u_p^{n-1} + \frac{\tau}{2m_p}\sum_{q\in N(p)} a_{pq}^{out}u_q^{n-1}\\
&= u_p^{n-1} + \frac{\tau}{2m_p}\sum_{q\in N(p)} a_{pq}^{out}u_p^n + \frac{\tau}{2m_p}\sum_{q\in N(p)} a_{pq}^{in}u_q^n\\
&\quad +\frac{\tau}{2m_p}\sum_{q\in N(p)} a_{pq}^{in}u_p^{n-1} + \frac{\tau}{2m_p}\sum_{q\in N(p)} a_{pq}^{out}u_q^{n-1}\\
&= u_p^{n-1} + \frac{\tau}{m_p}\sum_{q\in N(p)} \underbrace{a_{pq}^{in}\frac{1}{2}(u_q^n + u_p^{n-1})}_{=-g_{pq}^{in}} + \frac{\tau}{m_p}\sum_{q\in N(p)} \underbrace{a_{pq}^{out}\frac{1}{2}(u_p^n + u_q^{n-1})}_{=-g_{pq}^{out}}.
\end{aligned}$$

Let us consider that e_{pq} is an inflow boundary with respect to p, and hence an outflow boundary for q. With $a_{pq}^{in} = -a_{qp}^{out}$, we then obtain

$$g_{pq} + g_{qp} = g_{pq}^{in} + g_{qp}^{out} = -a_{pq}^{in}\frac{1}{2}(u_q^n + u_p^{n-1}) - \underbrace{a_{qp}^{out}}_{=-a_{pq}^{in}} \frac{1}{2}(u_q^n + u_p^{n-1}) = 0.$$

If e_{pq} is an outflow boundary with respect to p and inflow with respect to q, we analogously get

$$g_{pq} + g_{qp} = g_{pq}^{out} + g_{qp}^{in} = -a_{pq}^{out}\frac{1}{2}(u_p^n + u_q^{n-1}) - \underbrace{a_{qp}^{in}}_{=-a_{pq}^{out}} \frac{1}{2}(u_p^n + u_q^{n-1}) = 0.$$

This proofs the lemma. □

Note, that the property of local mass conservation gets lost for the stabilized versions of the scheme. However, by numerical experiments we see that the global mass error for smooth solutions vanishes with the same order h^2 as the solution error in case of S^{1}I^{2}OE scheme and with the much higher order h^4 for the S^{2}I^{2}OE scheme, cf. Table 5.2. The area error is negligible, for dense grids below machine precision, in case of moving discontinuities by linear advection, cf. Table 5.3.

Theorem 4.3 (Exactness for quadratic polynomials) *Let us consider equation* (1.1) *with constant velocity vector* $\mathbf{v}$ *and* I^{2}OE *scheme* (2.7) *on uniform rectangular grids with grid sizes h_i. Let the initial condition be given as a second order polynomial. Then the* I^{2}OE *scheme* (2.7) *gives the exact solution for any choice of time step τ.*

Proof. For simplicity let us first consider the 1D case. A general second order polynomial initial condition is of the form $u_0(x) = ax^2 + bx + c$ and exact solution at time τ is given by $u(x,\tau) = u^0(x - v\tau)$. With positive v the scheme (3.3) takes the form

$$u_i^n + \frac{\tau v}{2h}(u_i^n - u_{i-1}^n) = u_i^{n-1} - \frac{\tau(-v)}{2h}(u_i^{n-1} - u_{i+1}^{n-1}) \tag{4.1}$$

If we plug into the scheme (4.1) the exact values in grid points x_i, x_{i-1}, x_{i+1} at time steps $t^{n-1} = 0$ and $t^n = \tau$, namely

$$u_i^{n-1} = ax_i^2 + bx_i + c,\ u_{i+1}^{n-1} = a(x_i + h)^2 + b(x_i + h) + c, \tag{4.2}$$
$$u_i^n = a(x_i - v\tau)^2 + b(x_i - v\tau) + c,\ u_{i-1}^n = a(x_i - h - v\tau)^2 + b(x_i - h - v\tau) + c,$$

we end-up with true identity. In fact, it can be easily checked, e.g. by a symbolic computing system like Mathematica, that both sides are equal to $ax_i^2 + bx_i - av\tau x_i - \frac{1}{2}bv\tau - \frac{1}{2}ahv\tau + c$ and thus their difference is 0. In case of negative velocity v the scheme (3.3) takes the form

$$u_i^n + \frac{\tau(-v)}{2h}(u_i^n - u_{i+1}^n) = u_i^{n-1} - \frac{\tau v}{2h}(u_i^{n-1} - u_{i-1}^{n-1}) \tag{4.3}$$

and again plugging the exact values (4.2) into (4.3) give true identity, both sides are equal to $ax_i^2 + bx_i - av\tau x_i - \frac{1}{2}bv\tau + \frac{1}{2}ahv\tau + c$.

In the 3D case a general quadratic polynomial has the form $a_0 + a_1x + a_2y + a_3z + a_4xy + a_5xz + a_6yz + a_7x^2 + a_8y^2 + a_9z^2$. In Figure 4.1 we present symbolic Mathematica code for checking exactness of I^{2}OE in 3D on uniform rectangular grids. These calculations surely generalize to arbitrary space dimensions. □

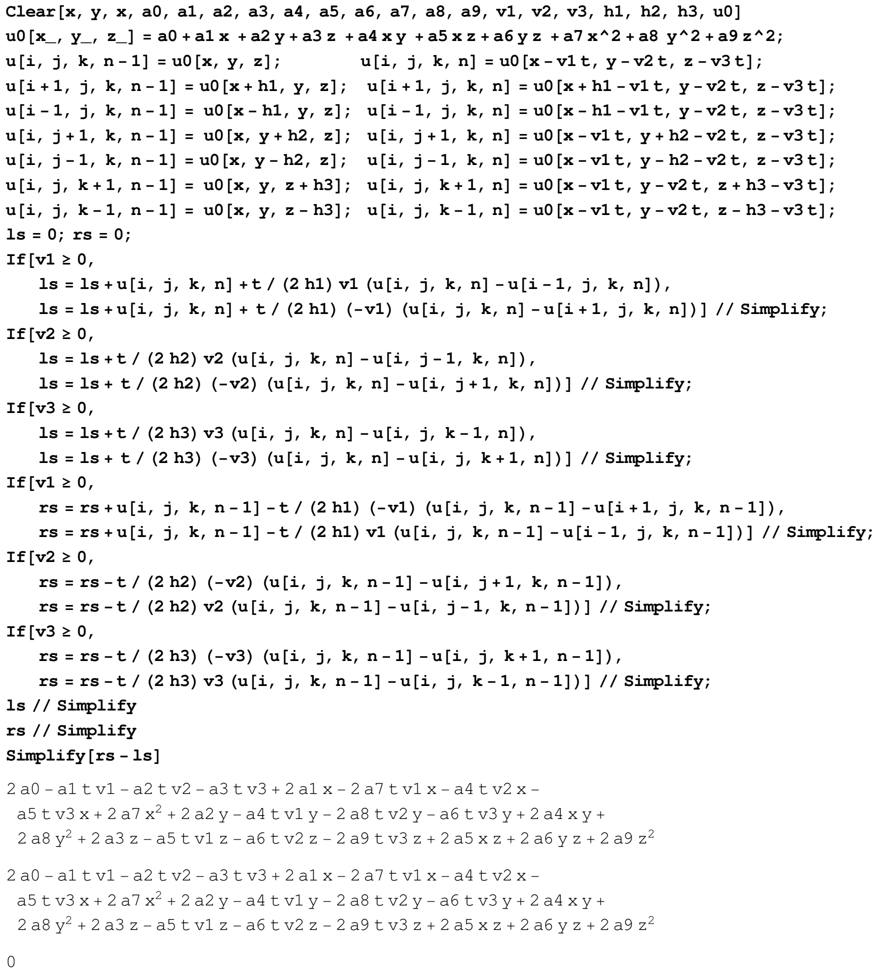

```
Clear[x, y, x, a0, a1, a2, a3, a4, a5, a6, a7, a8, a9, v1, v2, v3, h1, h2, h3, u0]
u0[x_, y_, z_] = a0 + a1 x + a2 y + a3 z + a4 x y + a5 x z + a6 y z + a7 x^2 + a8 y^2 + a9 z^2;
u[i, j, k, n - 1] = u0[x, y, z];         u[i, j, k, n] = u0[x - v1 t, y - v2 t, z - v3 t];
u[i + 1, j, k, n - 1] = u0[x + h1, y, z];  u[i + 1, j, k, n] = u0[x + h1 - v1 t, y - v2 t, z - v3 t];
u[i - 1, j, k, n - 1] = u0[x - h1, y, z];  u[i - 1, j, k, n] = u0[x - h1 - v1 t, y - v2 t, z - v3 t];
u[i, j + 1, k, n - 1] = u0[x, y + h2, z];  u[i, j + 1, k, n] = u0[x - v1 t, y + h2 - v2 t, z - v3 t];
u[i, j - 1, k, n - 1] = u0[x, y - h2, z];  u[i, j - 1, k, n] = u0[x - v1 t, y - h2 - v2 t, z - v3 t];
u[i, j, k + 1, n - 1] = u0[x, y, z + h3];  u[i, j, k + 1, n] = u0[x - v1 t, y - v2 t, z + h3 - v3 t];
u[i, j, k - 1, n - 1] = u0[x, y, z - h3];  u[i, j, k - 1, n] = u0[x - v1 t, y - v2 t, z - h3 - v3 t];
ls = 0; rs = 0;
If[v1 ≥ 0,
   ls = ls + u[i, j, k, n] + t / (2 h1) v1 (u[i, j, k, n] - u[i - 1, j, k, n]),
   ls = ls + u[i, j, k, n] + t / (2 h1) (-v1) (u[i, j, k, n] - u[i + 1, j, k, n])] // Simplify;
If[v2 ≥ 0,
   ls = ls + t / (2 h2) v2 (u[i, j, k, n] - u[i, j - 1, k, n]),
   ls = ls + t / (2 h2) (-v2) (u[i, j, k, n] - u[i, j + 1, k, n])] // Simplify;
If[v3 ≥ 0,
   ls = ls + t / (2 h3) v3 (u[i, j, k, n] - u[i, j, k - 1, n]),
   ls = ls + t / (2 h3) (-v3) (u[i, j, k, n] - u[i, j, k + 1, n])] // Simplify;
If[v1 ≥ 0,
   rs = rs + u[i, j, k, n - 1] - t / (2 h1) (-v1) (u[i, j, k, n - 1] - u[i + 1, j, k, n - 1]),
   rs = rs + u[i, j, k, n - 1] - t / (2 h1) v1 (u[i, j, k, n - 1] - u[i - 1, j, k, n - 1])] // Simplify;
If[v2 ≥ 0,
   rs = rs - t / (2 h2) (-v2) (u[i, j, k, n - 1] - u[i, j + 1, k, n - 1]),
   rs = rs - t / (2 h2) v2 (u[i, j, k, n - 1] - u[i, j - 1, k, n - 1])] // Simplify;
If[v3 ≥ 0,
   rs = rs - t / (2 h3) (-v3) (u[i, j, k, n - 1] - u[i, j, k + 1, n - 1]),
   rs = rs - t / (2 h3) v3 (u[i, j, k, n - 1] - u[i, j, k - 1, n - 1])] // Simplify;
ls // Simplify
rs // Simplify
Simplify[rs - ls]

2 a0 - a1 t v1 - a2 t v2 - a3 t v3 + 2 a1 x - 2 a7 t v1 x - a4 t v2 x -
 a5 t v3 x + 2 a7 x^2 + 2 a2 y - a4 t v1 y - 2 a8 t v2 y - a6 t v3 y + 2 a4 x y +
 2 a8 y^2 + 2 a3 z - a5 t v1 z - a6 t v2 z - 2 a9 t v3 z + 2 a5 x z + 2 a6 y z + 2 a9 z^2

2 a0 - a1 t v1 - a2 t v2 - a3 t v3 + 2 a1 x - 2 a7 t v1 x - a4 t v2 x -
 a5 t v3 x + 2 a7 x^2 + 2 a2 y - a4 t v1 y - 2 a8 t v2 y - a6 t v3 y + 2 a4 x y +
 2 a8 y^2 + 2 a3 z - a5 t v1 z - a6 t v2 z - 2 a9 t v3 z + 2 a5 x z + 2 a6 y z + 2 a9 z^2

0
```

FIG. 4.1. *Mathematica code for algebraic evaluation of the* I^{2}OE *scheme on uniform rectangular 3D grid for a general second order polynomial.*

Theorem 4.4 (Formal second order consistency) *Let us consider the equation* (1.1) *in 1D with variable smooth velocity and the* I^{2}OE *scheme* (3.3) *on a uniform grid. Then the scheme is formally second order and the consistency error is of order* $\mathcal{O}(h^2) + \mathcal{O}(\tau h) + \mathcal{O}(\tau^2)$.

Proof. As the scheme depends on inflow/outflow properties of the cell boundaries, we have to distinguish four cases: a) $v_{i-1/2}, v_{i+1/2} \geq 0$, b) $v_{i-1/2}, v_{i+1/2} \leq 0$, c) $v_{i-1/2} < 0, v_{i+1/2} > 0$, and d) $v_{i-1/2}{>}0, v_{i+1/2}{<}0$. In both cases, a) and b), we have one inflow and one outflow cell boundary, while in case c) we have only outflows and in d) only inflows.

Let us first look at the cases a) and b). We write our transport equation as $\partial_t u + f(v, \partial_x u) = 0$ with $f(v, \partial_x u) := v(x)\partial_x u$. We will use notations $u^n := u(t^n)$, $f^n := f(v, \partial_x u^n)$. The Taylor expansion in time yields

$$u^n = u^{n-1} + \tau \partial_t u^{n-1} + \frac{\tau^2}{2}\partial_t^2 u^{n-1} + \mathcal{O}(\tau^3), \quad u^{n-1} = u^n - \tau \partial_t u^n + \frac{\tau^2}{2}\partial_t^2 u^n + \mathcal{O}(\tau^3).$$

Subtracting these two equations we derive relation

$$u^n - u^{n-1} = \frac{\tau}{2}(\partial_t u^n + \partial_t u^{n-1}) + \frac{\tau^2}{4}(\partial_t^2 u^{n-1} - \partial_t^2 u^n) + \mathcal{O}(\tau^3). \tag{4.4}$$

We can see that the second term on the right hand side is also $\mathcal{O}(\tau^3)$ and using the equation $\partial_t u + f(v, \partial_x u) = 0$, we get for the first term of the right hand side

$$I = \frac{\tau}{2}(\partial_t u^n + \partial_t u^{n-1}) = -\frac{\tau}{2}(f^n + f^{n-1}) \tag{4.5}$$

Using the notation $f_i := f(x_i) = v(x_i)\partial_x u(x_i)$, by the Taylor expansion in space we have for case a)

$$f^n_{i-1/2} = f^n_i - \frac{h}{2}\partial_x f^n_i + \mathcal{O}(h^2), \quad f^{n-1}_{i+1/2} = f^{n-1}_i + \frac{h}{2}\partial_x f^{n-1}_i + \mathcal{O}(h^2) \tag{4.6}$$

or for case b)

$$f^{n-1}_{i-1/2} = f^{n-1}_i - \frac{h}{2}\partial_x f^{n-1}_i + \mathcal{O}(h^2), \quad f^n_{i+1/2} = f^n_i + \frac{h}{2}\partial_x f^n_i + \mathcal{O}(h^2) \tag{4.7}$$

We continue for case a). Using (4.5)-(4.6) we derive

$$I_i = -\frac{\tau}{2}(f^n_i + f^{n-1}_i) = -\frac{\tau}{2}\Big(f^n_{i-1/2} + f^{n-1}_{i+1/2} + \frac{h}{2}(\partial_x f^n_i - \partial_x f^{n-1}_i) + \mathcal{O}(h^2)\Big).$$

The term $\frac{h}{2}(\partial_x f^n_i - \partial_x f^{n-1}_i)$ in the brackets on the right hand side is of order $\mathcal{O}(\tau h)$ and we shall analyse the term $f^n_{i-1/2} + f^{n-1}_{i+1/2}$. We know that

$$\partial_x u^n_{i-1/2} = \frac{1}{h}(u^n_i - u^n_{i-1}) + \mathcal{O}(h^2), \quad \partial_x u^{n-1}_{i+1/2} = \frac{1}{h}(u^{n-1}_{i+1} - u^{n-1}_i) + \mathcal{O}(h^2)$$

and resubstituting for $f^n_{i-1/2} = v_{i-1/2}\partial_x u^n_{i-1/2}$ and $f^{n-1}_{i+1/2} = v_{i+1/2}\partial_x u^{n-1}_{i+1/2}$ we get

$$I_i = -\frac{\tau}{2}\Big(v_{i-1/2}\frac{1}{h}(u^n_i - u^n_{i-1}) + v_{i+1/2}\frac{1}{h}(u^{n-1}_{i+1} - u^{n-1}_i)\Big) + \mathcal{O}(\tau^2 h) + \mathcal{O}(\tau h^2). \tag{4.8}$$

From (4.4) and (4.8) we finally get

$$\begin{aligned} u^n_i - u^{n-1}_i = &-\frac{\tau}{2}\Big(\frac{v_{i-1/2}}{h}(u^n_i - u^n_{i-1}) + \frac{v_{i+1/2}}{h}(u^{n-1}_{i+1} - u^{n-1}_i)\Big) \\ &+ \mathcal{O}(\tau^2 h) + \mathcal{O}(\tau h^2) + \mathcal{O}(\tau^3) \end{aligned}$$

where we recognize the scheme (3.3) for case a), cf. also (4.1), and dividing by τ we get the consistency error of the I^{2}OE scheme stated in the theorem. The result for case b) follows analogously to a), using (4.7) instead of (4.6).

The cases c) and d) have to be treated differently, as in c) only explicit fluxes and in d) only implicit fluxes are used in the scheme. Let us start with case c). We start from Taylor expansion in time with only explicit evaluations of time derivatives.

$$u^n - u^{n-1} = \tau\partial_t u^{n-1} + \frac{\tau^2}{2}\partial_t^2 u^{n-1} + \mathcal{O}(\tau^3). \tag{4.9}$$

With the expansion of the explicit fluxes

$$f^{n-1}_{i-1/2} = f^{n-1}_i - \frac{h}{2}\partial_x f^{n-1}_i + \mathcal{O}(h^2), \quad f^{n-1}_{i+1/2} = f^{n-1}_i + \frac{h}{2}\partial_x f^{n-1}_i + \mathcal{O}(h^2) \tag{4.10}$$

we now obtain using $\partial_t u + f(v, \partial_x u) = 0$,

$$\tau \partial_t u_i^{n-1} = -\tau f_i^{n-1} = -\frac{\tau}{2}(f_{i-1/2}^{n-1} + f_{i+1/2}^{n-1} + \mathcal{O}(h^2)) \tag{4.11}$$

Next, we will show that the term $\frac{\tau^2}{2}\partial_t^2 u^{n-1}$ of (4.9) is actually $\mathcal{O}(\tau^2 h)$ due to the smallness of the velocity in this case. Using $\partial_t u + f(v, \partial_x u) = 0$, we get

$$\partial_t^2 u_i^{n-1} = \partial_t f_i^{n-1} = v_i \partial_t \partial_x u_i^{n-1}. \tag{4.12}$$

As the velocity field is smooth and changes sign within the cell $(x_{i-1/2}, x_{i+1/2}$, there exists some $x^\star \in (x_{i-1/2}, x_{i+1/2})$ with $v(x^\star) = 0$. Hence, by Taylor expansion we get

$$v_i = v(x_i) = \underbrace{v(x^\star)}_{=0} + (x_i - x^\star)\partial_x v(x^\star) + \mathcal{O}(h^2).$$

Thus, we have $v_i = \mathcal{O}(h)$ and we obtain

$$\frac{\tau^2}{2}\partial_t^2 u_i^{n-1} = \frac{\tau^2}{2} v_i \partial_t \partial_x u_i^{n-1} = \mathcal{O}(\tau^2 h). \tag{4.13}$$

Together with (4.9) and (4.11) we thus obtain the result, i.e.

$$u^n - u^{n-1} = -\frac{\tau}{2}(f_{i-1/2}^{n-1} + f_{i+1/2}^{n-1}) + \mathcal{O}(\tau h^2) + \mathcal{O}(\tau^2 h) + \mathcal{O}(\tau^3).$$

Case d) is obtained analogously to c) by using Taylor expansion in time with only implicit evaluations of time derivatives and replacing the explicit fluxes by corresponding implicit ones. □

Theorem 4.5 ($\mathbf{L^\infty(L^2)}$ stability) *Let us consider the advection equation in 1D with constant velocity $v \geq 0$ (or $v \leq 0$) and the* I^{2}OE *scheme on a uniform grid with periodic boundary conditions. Then the scheme is L^2 stable and the following a priori estimate holds*

$$\sum_{i\in I}\int_{p_i}(u_i^N)^2 + \sum_{i\in I}\int_{p_i}\frac{|v|\tau}{4h}(u_i^N - u_{i-1}^N)^2 = \sum_{i\in I}\int_{p_i}(u_i^0)^2 + \sum_{i\in I}\int_{p_i}\frac{|v|\tau}{4h}(u_{i+1}^0 - u_i^0)^2.$$

Proof. Without loss of generality, let us assume constant velocity $v \geq 0$. The basic I^{2}OE scheme then reads

$$\frac{u_i^n - u_i^{n-1}}{\tau} + \frac{1}{2}v\Big(\frac{u_i^n - u_{i-1}^n}{h} + \frac{u_{i+1}^{n-1} - u_i^{n-1}}{h}\Big) = 0,$$

where $i \in I$, $n = 1, ..., N$, I is the number of finite volumes and N is the number of time steps. Testing with $\frac{1}{2}(u_i^n + u_i^{n-1})$ yields after integration over cell p_i and time interval (t^n, t^{n+1}) and summation

$$\sum_{n=1}^{N}\sum_{i\in I}\int_{t^n}^{t^{n+1}}\int_{p_i}(T_t + T_s) = 0, \tag{4.14}$$

where the time and space terms are given as

$$T_t := \frac{1}{2\tau}(u_i^n - u_i^{n-1})(u_i^n + u_i^{n-1}) = \frac{1}{2\tau}\Big((u_i^n)^2 - (u_i^{n-1})^2\Big), \tag{4.15}$$

$$T_s := \frac{v}{4h}\Big((u_i^n - u_{i-1}^n) + (u_{i+1}^{n-1} - u_i^{n-1})\Big)(u_i^n + u_i^{n-1}). \tag{4.16}$$

By simple algebraic manipulation, we further get for T_s

$$\begin{aligned}T_s &= \frac{v}{8h}\Big((u_i^n - u_{i-1}^n) + (u_{i+1}^{n-1} - u_i^{n-1})\Big)\Big((u_i^n - u_{i-1}^n) - (u_{i+1}^{n-1} - u_i^{n-1})\Big)\\ &+ \frac{v}{8h}\Big((u_i^n + u_{i+1}^{n-1}) - (u_{i-1}^n + u_i^{n-1})\Big)\Big((u_i^n + u_{i+1}^{n-1}) + (u_{i-1}^n + u_i^{n-1})\Big)\\ &= \frac{v}{8h}\Big(\underbrace{(u_i^n - u_{i-1}^n)^2}_{=:(\Delta_{i-1}^n)^2} - \underbrace{(u_{i+1}^{n-1} - u_i^{n-1})^2}_{=:(\Delta_i^{n-1})^2} + \underbrace{(u_i^n + u_{i+1}^{n-1})^2}_{=:(S_i^{n+1/2})^2} - \underbrace{(u_{i-1}^n + u_i^{n-1})^2}_{=:(S_{i-1}^{n+1/2})^2}\Big).\end{aligned}$$

In this form of the space term, it can be seen that the term $(\Delta_i^{n-1})^2$ is a space-time shift of $(\Delta_{i-1}^n)^2$, and $(S_i^{n+1/2})^2$ is a space shift of $(S_{i-1}^{n+1/2})^2$. We thus obtain from (4.14) with periodicity and using the shift correlation in the T_t and T_s-terms

$$0 = \sum_{i\in I}\int_{p_i}\frac{1}{2}\Big((u_i^N)^2 - (u_i^0)^2\Big) + \sum_{i\in I}\int_{p_i}\frac{v\tau}{8h}\Big((\Delta_{i-1}^N)^2 - (\Delta_i^0)^2\Big). \tag{4.17}$$

Hence, we obtain with the definition of the Δ-terms

$$\sum_{i\in I}\int_{p_i}(u_i^N)^2 + \sum_{i\in I}\int_{p_i}\frac{v\tau}{4h}(u_i^N - u_{i-1}^N)^2 = \sum_{i\in I}\int_{p_i}(u_i^0)^2 + \sum_{i\in I}\int_{p_i}\frac{v\tau}{4h}(u_{i+1}^0 - u_i^0)^2.$$

As the proof of the stability estimate only relies on space and time shifts, it transfers immediately also to the case of uniform rectangular grids in multiple space dimensions. □

Theorem 4.6 ($\mathbf{L}^\infty(\mathbf{L}^\infty)$ stability of the stabilized $\mathbf{I}^2$OE schemes) *Let us consider the advection equation (1.1) with given variable velocity. Then, the stabilized* S^{1}I^{2}OE *and* S^{2}I^{2}OE *schemes are unconditionally stable in the $L^\infty(L^\infty)$ sense and the following minimum-maximum property holds*

$$\min_{q\in\mathcal{T}_h} u_q^0 \le u_p^n \le \max_{q\in\mathcal{T}_h} u_q^0, \quad \forall q \in \mathcal{T}_h, n = 0,\dots,N. \tag{4.18}$$

Proof. The theorem follows from the construction of the stabilized I^{2}OE schemes as discussed in Section 2 above. □

5. Numerical experiments. This section is devoted to numerically analyze and validate the robustness and accuracy of our new I^{2}OE scheme at classical benchmark problems and more involved multi-dimensional applications. We start the evaluation with one dimensional advection with constant speed of a quadratic polynomial, a smooth hump and discontinuous piecewise constant initial data. For each case we compare our new basic and stabilized methods with the classical implicit up-wind scheme and the implicit up-wind Gear's scheme. Here we are in particular interested in an evaluation of the methods when large time steps are used that exceed the time step given from the CFL condition. For further one dimensional experiments involving also advection with non divergence free velocity and for comparison with higher order explicit methods we refer to the exposition in [13, 14]. Finally, the last part of this section will be devoted to two dimensional benchmark problems and an evaluation of the scheme for real applications in medical image segmentation.

Table 5.1

Case a) $L^1(I, L^1)$ errors of the I^{2}OE , S^{1}I^{2}OE, S^{2}I^{2}OE, *implicit up-wind, and Gear's up-wind schemes for advection of a quadratic polynomial. The relation $\tau = h$ is used in the first 4 rows, $\tau = h/2$ in the next 4 rows, $\tau = 2h$ in the next 4 rows, $\tau = 10h$ in the next 4 rows and the last 5 rows report the errors for fixed $n = 160$ and refining time step from $\tau = 80h$ to $\tau = 5h$.*

n	NTS	I^{2}OE	S^{1}I^{2}OE	S^{2}I^{2}OE	implicit up-wind	Gear's scheme
20	10	$1.8\ 10^{-16}$	$4.63\ 10^{-3}$	$3.8\ 10^{-16}$	$8.80\ 10^{-2}$	$5.56\ 10^{-2}$
40	20	$3.5\ 10^{-16}$	$1.18\ 10^{-3}$	$4.9\ 10^{-16}$	$4.28\ 10^{-2}$	$2.44\ 10^{-2}$
80	40	$7.5\ 10^{-16}$	$3.12\ 10^{-4}$	$6.3\ 10^{-16}$	$2.11\ 10^{-2}$	$1.13\ 10^{-2}$
160	80	$1.4\ 10^{-15}$	$8.35\ 10^{-5}$	$7.2\ 10^{-16}$	$1.05\ 10^{-2}$	$5.44\ 10^{-3}$
20	20	$3.7\ 10^{-16}$	$1.75\ 10^{-3}$	$5.2\ 10^{-16}$	$6.43\ 10^{-2}$	$4.61\ 10^{-2}$
40	40	$8.0\ 10^{-16}$	$4.60\ 10^{-4}$	$5.1\ 10^{-16}$	$3.17\ 10^{-2}$	$2.20\ 10^{-2}$
80	80	$1.1\ 10^{-15}$	$1.23\ 10^{-4}$	$7.9\ 10^{-16}$	$1.57\ 10^{-2}$	$1.07\ 10^{-2}$
160	160	$2.4\ 10^{-15}$	$3.22\ 10^{-5}$	$1.2\ 10^{-15}$	$0.78\ 10^{-2}$	$5.28\ 10^{-3}$
20	5	$2.1\ 10^{-16}$	$1.12\ 10^{-2}$	$1.9\ 10^{-16}$	$1.38\ 10^{-1}$	$8.70\ 10^{-2}$
40	10	$2.1\ 10^{-16}$	$2.77\ 10^{-3}$	$2.1\ 10^{-16}$	$6.60\ 10^{-2}$	$3.31\ 10^{-2}$
80	20	$3.9\ 10^{-16}$	$7.04\ 10^{-4}$	$2.6\ 10^{-16}$	$3.21\ 10^{-2}$	$1.35\ 10^{-2}$
160	40	$5.7\ 10^{-16}$	$1.80\ 10^{-4}$	$4.1\ 10^{-16}$	$1.58\ 10^{-2}$	$6.01\ 10^{-3}$
20	1	$4.3\ 10^{-16}$	$2.18\ 10^{-1}$	$6.4\ 10^{-16}$	$6.31\ 10^{-1}$	$6.31\ 10^{-1}$
40	2	$1.0\ 10^{-15}$	$4.91\ 10^{-2}$	$8.5\ 10^{-16}$	$2.8\ 10^{-1}$	$2.20\ 10^{-1}$
80	4	$1.5\ 10^{-15}$	$1.13\ 10^{-2}$	$1.8\ 10^{-15}$	$1.29\ 10^{-1}$	$7.12\ 10^{-2}$
160	8	$2.5\ 10^{-15}$	$2.66\ 10^{-3}$	$3.1\ 10^{-15}$	$0.61\ 10^{-1}$	$2.19\ 10^{-2}$
160	1	$2.6\ 10^{-15}$	$2.11\ 10^{-1}$	$1.2\ 10^{-15}$	$5.75\ 10^{-1}$	$5.75\ 10^{-1}$
160	2	$2.6\ 10^{-15}$	$4.62\ 10^{-2}$	$2.7\ 10^{-15}$	$2.61\ 10^{-1}$	$2.00\ 10^{-1}$
160	4	$2.6\ 10^{-15}$	$1.07\ 10^{-2}$	$3.5\ 10^{-15}$	$1.23\ 10^{-1}$	$6.51\ 10^{-2}$
160	8	$2.6\ 10^{-15}$	$2.66\ 10^{-3}$	$3.1\ 10^{-15}$	$6.12\ 10^{-2}$	$2.19\ 10^{-2}$
160	16	$2.6\ 10^{-15}$	$7.31\ 10^{-4}$	$4.6\ 10^{-15}$	$3.23\ 10^{-2}$	$9.71\ 10^{-3}$

5.1. 1D advection with constant velocity.

As a classical benchmark let us consider one dimensional advection with constant speed given by equation (3.1) with $v(x) \equiv 1$. In all our computations, we restrict to the space interval $\Omega = (-1, 1)$ and time interval $I = (0, T)$ with $T = 1$. We consider three representative examples in this subsection:

a) advection of the quadratic polynomial $u_0(x) = 1 - \frac{1}{2}(x^2 + x)$,

b) advection of a smooth hump defined as $u_0(x) = \max(0, \cos^5(\pi(x + 0.5)))$, and

c) advection of a discontinuous piecewise constant profile given as $u_0(x) = 1$ for $x \in [-0.75, -0.25]$ and $u_0(x) = 0$ otherwise.

The exact solution for all these examples is given by shifting in time the initial profile, i.e. $u(x, t) = u_0(x - vt)$.

Case a) As proven in Section 4, the basic I^{2}OE is exact for advection of a quadratic polynomial. This is of course also seen numerically up to machine accuracy, as depicted in the third column of Table 5.1. However, exactness is not the case for the stabilized S^{1}I^{2}OE scheme, which is just second order, but it is again true for the stabilized S^{2}I^{2}OE scheme, cf. fourth and fifth column of Table 5.1. The fully implicit up-wind scheme is only first order and Gear's scheme shows only slightly higher order than 1 for a coupling $\tau = Ch$ with C moderately bigger than 1, while it shows order about 1.5 for fine grids and large time steps (cf. last two columns of Table 5.1).

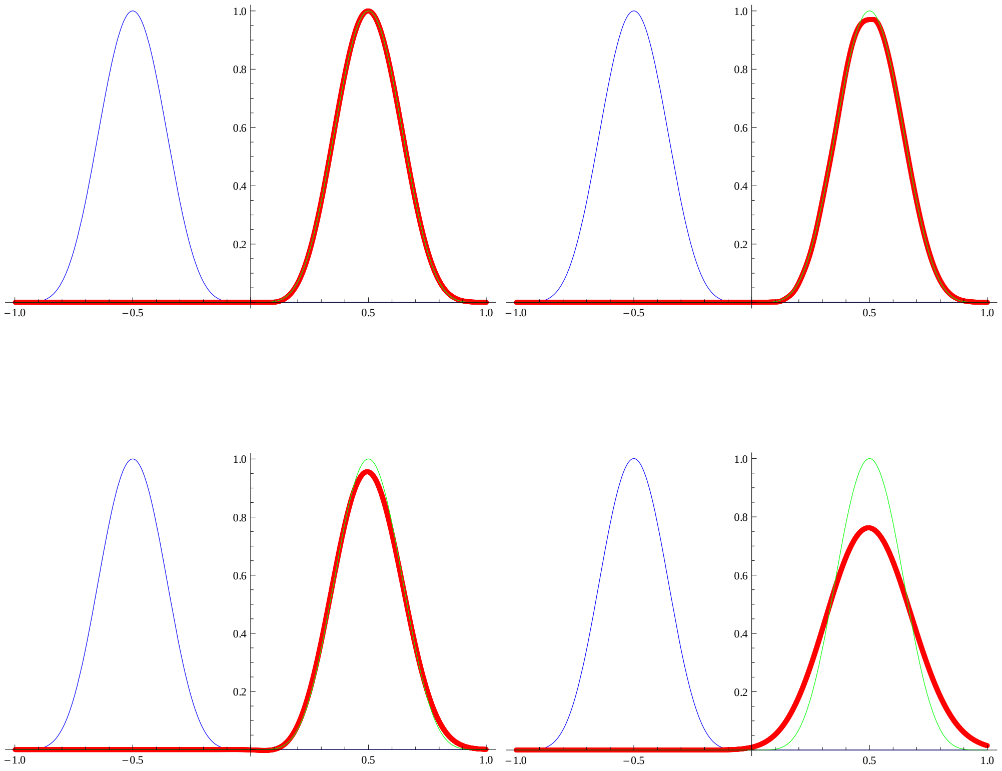

FIG. 5.1. *Case b) Smooth initial data (blue curves), exact solution (green curves), and numerical results at $T = 1$ (red curves) for the stabilized schemes with quadratic reconstruction* $\mathrm{S^2I^2OE}$*(top left),* $\mathrm{S^1I^2OE}$ *(top right) in comparison to the results with Gear's up-wind scheme (bottom left) and implicit up-wind scheme (bottom right). For these computations, $n = 1280$ and the relation $\tau = 8h$ is used, i.e. CFL $= 8$.*

In all cases, the $\mathrm{S^1I^2OE}$ absolute errors are about one order less than the errors of the two up-wind implicit schemes. Clearly the $\mathrm{S^2I^2OE}$ scheme is superior because it conserves the exactness of the quadratic solution for time steps given by an integer multiplication of h and when using local quadratic reconstruction also for time steps less than h, cf. Table 5.1.

Case b) For the more general smooth profile we analyze both, the accuracy and the local mass conservation error (area error) of the respective stabilized $\mathrm{I^2OE}$ schemes. For smooth solutions we observe that the $\mathrm{S^2I^2OE}$ scheme with quadratic reconstruction behaves similar as the basic $\mathrm{I^2OE}$ scheme, while the $\mathrm{S^1I^2OE}$ scheme with quadratic reconstruction stabilizes a bit more and thus shows slightly worse accuracy in the L^1 error and the area error. We also compare the new stabilized schemes with the up-wind implicit and Gear's up-wind schemes. A visual comparison of all these methods is shown in Figure 5.1. While the $\mathrm{S^2I^2OE}$ scheme shows visually perfect matching with the exact solution, there is a little bit more smearing of the hump for the $\mathrm{S^1I^2OE}$ scheme. However, both new methods show better accuracy as the implicit Gear's scheme and much better behavior as the very dissipative classical implicit up-wind scheme. The visual comparison is detailed in the convergence study

Table 5.2

Case b) Report on the $L^1(I, L^1)$ and area errors of the S^{1}I^{2}OE, S^{2}I^{2}OE *schemes (with quadratic reconstruction) and $L^1(I, L^1)$ errors of the implicit up-wind and Gear's up-wind schemes. The relation $\tau = h$ is used in the first 6 rows and $\tau = 8h$ in the next 4 rows.*

						implicit	Gear's
		S^{1}I^{2}OE	S^{1}I^{2}OE	S^{2}I^{2}OE	S^{2}I^{2}OE	up-wind	scheme
n	NTS	L^1-error	area error	L^1-error	area error	L^1-error	L^1-error
40	20	9.53 10^{-2}	6.69 10^{-2}	9.19 10^{-2}	1.93 10^{-2}	1.96 10^{-1}	1.49 10^{-1}
80	40	3.51 10^{-2}	6.58 10^{-3}	2.80 10^{-2}	2.98 10^{-3}	1.32 10^{-1}	8.82 10^{-2}
160	80	9.66 10^{-3}	2.06 10^{-3}	7.69 10^{-3}	2.69 10^{-4}	8.21 10^{-2}	4.90 10^{-2}
320	160	2.69 10^{-3}	6.26 10^{-4}	1.97 10^{-3}	1.94 10^{-5}	4.71 10^{-2}	2.61 10^{-2}
640	320	7.00 10^{-4}	1.63 10^{-4}	4.97 10^{-4}	1.28 10^{-6}	2.56 10^{-2}	1.35 10^{-2}
1280	640	1.80 10^{-4}	4.16 10^{-5}	1.24 10^{-4}	8.14 10^{-8}	1.33 10^{-2}	6.89 10^{-3}
640	40	1.03 10^{-2}	2.96 10^{-3}	7.23 10^{-3}	2.81 10^{-4}	9.02 10^{-2}	2.83 10^{-2}
1280	80	2.77 10^{-3}	7.75 10^{-4}	1.86 10^{-3}	2.03 10^{-5}	5.23 10^{-2}	1.03 10^{-2}
2560	160	7.12 10^{-4}	1.94 10^{-4}	4.67 10^{-4}	1.32 10^{-6}	2.86 10^{-2}	4.21 10^{-3}
5120	320	1.82 10^{-4}	4.81 10^{-5}	1.16 10^{-4}	8.35 10^{-8}	1.49 10^{-2}	1.91 10^{-3}

Table 5.3

Case c) Report on the $L^1(I, L^1)$ and area errors of the S^{1}I^{2}OE, S^{2}I^{2}OE *schemes with quadratic reconstruction and on the $L^1(I, L^1)$ errors of the implicit up-wind and Gear's up-wind schemes. The relation $\tau = h$ is used in the first 6 rows and $\tau = 8h$ in the next 4 rows.*

						implicit	Gear's
		S^{1}I^{2}OE	S^{1}I^{2}OE	S^{2}I^{2}OE	S^{2}I^{2}OE	up-wind	scheme
n	NTS	L^1-error	area error	L^1-error	area error	L^1-error	L^1-error
40	20	2.03 10^{-1}	1.06 10^{-3}	2.02 10^{-1}	6.17 10^{-4}	3.25 10^{-1}	2.57 10^{-1}
80	40	1.31 10^{-1}	5.32 10^{-5}	1.30 10^{-1}	5.09 10^{-5}	2.37 10^{-1}	1.77 10^{-1}
160	80	8.38 10^{-2}	5.47 10^{-7}	8.38 10^{-2}	5.47 10^{-7}	1.68 10^{-1}	1.23 10^{-1}
320	160	5.35 10^{-2}	5.69 10^{-10}	5.34 10^{-2}	5.68 10^{-10}	1.19 10^{-1}	8.55 10^{-2}
640	320	3.41 10^{-2}	3.34 10^{-15}	3.41 10^{-2}	3.33 10^{-15}	8.42 10^{-2}	5.99 10^{-2}
1280	640	2.16 10^{-2}	4.28 10^{-16}	2.16 10^{-2}	4.24 10^{-16}	5.95 10^{-2}	4.22 10^{-2}
640	40	9.22 10^{-2}	4.22 10^{-7}	9.22 10^{-2}	4.22 10^{-7}	1.79 10^{-1}	1.16 10^{-1}
1280	80	5.74 10^{-2}	3.77 10^{-10}	5.74 10^{-2}	3.77 10^{-10}	1.27 10^{-1}	7.54 10^{-2}
2560	160	3.58 10^{-2}	4.01 10^{-15}	3.58 10^{-2}	4.29 10^{-15}	8.95 10^{-2}	4.88 10^{-2}
5120	320	2.24 10^{-2}	4.96 10^{-15}	2.24 10^{-2}	2.60 10^{-14}	6.32 10^{-2}	3.14 10^{-2}

with respect to the solution, and, for the new schemes, with respect to the mass conservation error in Table 5.2. It can be seen that both stabilized I^{2}OE schemes show second order convergence, both for small ($\tau = h$) and large ($\tau = 8h$) time step sizes. The mass conservation error also converges to zero with second order for the S^{1}I^{2}OE, while it shows higher then fourth order convergence for the S^{1}I^{2}OE scheme. As expected, the implicit up-wind scheme is only first order, while Gear's up-wind scheme shows first order convergence for small time steps and slightly higher order (around 1.4) for larger time step sizes (cf. last two columns of Table 5.2).

Case c) Finally, we compare our methods for the discontinuous piecewise constant initial profile. Similar as in case b), Table 5.3 shows the detailed convergence behavior of the stabilized S^{1}I^{2}OE, and S^{2}I^{2}OE schemes with quadratic reconstruction. First of all, it can be observed that in this case both new stabilized schemes show

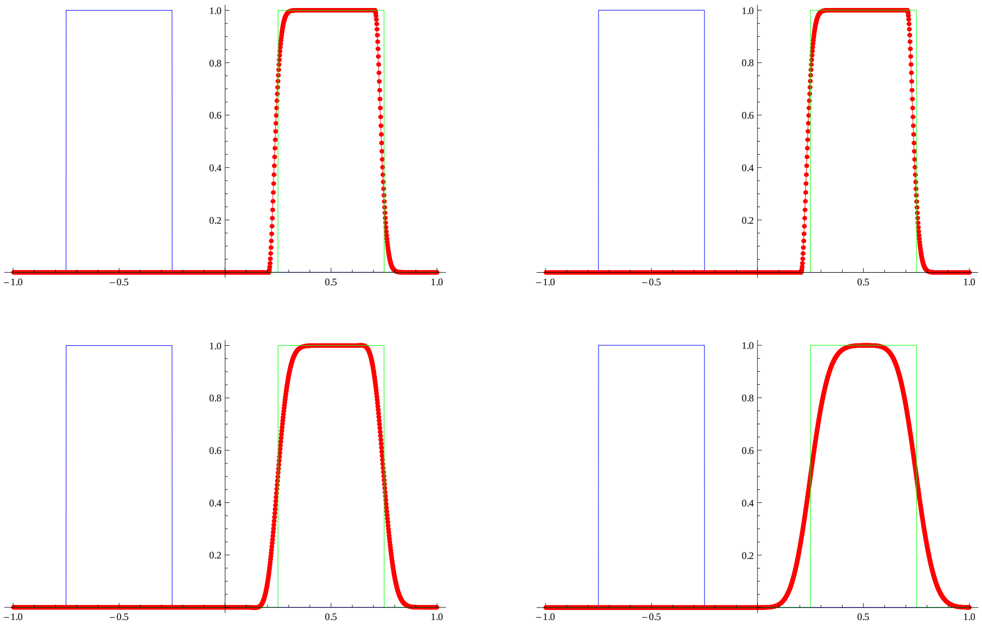

FIG. 5.2. *Case c) Results of the* $\mathrm{S}^2\mathrm{I}^2\mathrm{OE}$ *(with quadratic reconstruction) (top left) and* $\mathrm{S}^2\mathrm{I}^2\mathrm{OE}$ *(without quadratic reconstruction) (top right) schemes, Gear's up-wind (bottom left) and implicit up-wind (bottom right) schemes. The initial profile is given in blue, the exact solution in green, and the numerical solution in red. We used* $n = 1280$ *and the relation* $\tau = 2h$*.*

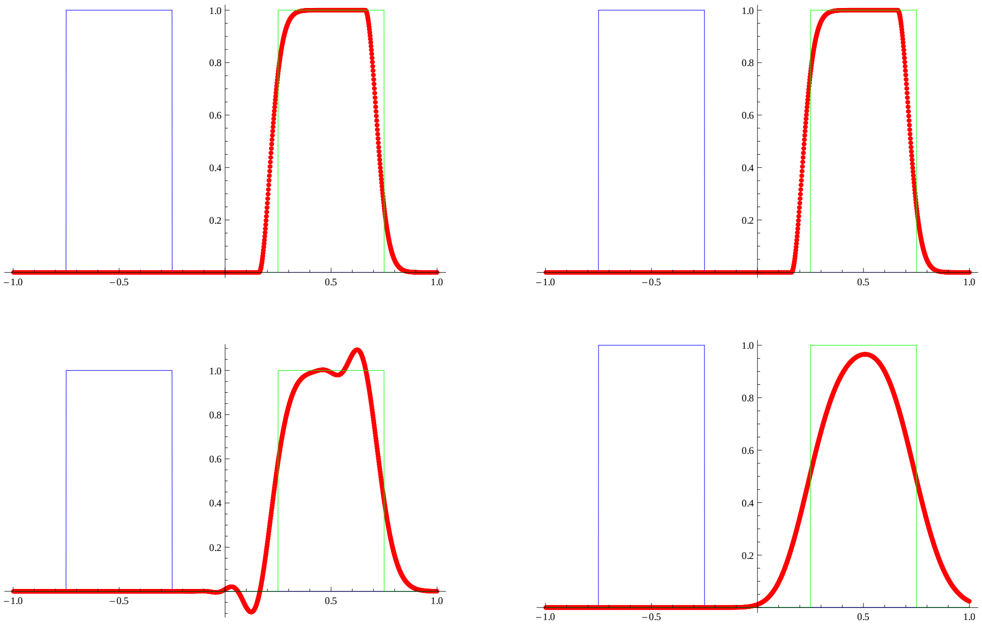

FIG. 5.3. *Case c) Here, the same comparison as in Figure 5.2 is plotted for larger choice of the time step size, i.e. we used* $n = 1280$ *and the relation* $\tau = 8h$*.*

Table 5.4
2D centered paraboloid rotated around the origin: report on the $L^1(I, L^1)$ errors of the I^{2}OE, S^{1}I^{2}OE, *and* S^{2}I^{2}OE *methods for refined space and time step sizes.*

n	τ	NTS	I^{2}OE $L^1(I, L^1)$	S^{1}I^{2}OE $L^1(I, L^1)$	S^{2}I^{2}OE $L^1(I, L^1)$
20	0.1	10	$5.938\ 10^{-16}$	$5.938\ 10^{-16}$	$5.938\ 10^{-16}$
40	0.05	20	$7.388\ 10^{-16}$	$7.388\ 10^{-16}$	$7.388\ 10^{-16}$
80	0.025	40	$1.079\ 10^{-15}$	$1.079\ 10^{-15}$	$1.079\ 10^{-15}$
160	0.0125	80	$1.367\ 10^{-15}$	$1.367\ 10^{-15}$	$1.367\ 10^{-15}$

approximately the same convergence behavior. Moreover, also the absolute errors in the solution and with respect to mass conservation are nearly the same. In this non-smooth example, the experimental order of convergence is about 2/3 for both stabilized I^{2}OE schemes, while it is only about 1/2 for the classical implicit up-wind scheme and Gear's up-wind scheme. For Gear's up-wind scheme the experimental order of convergence increases to about 0.62 in the case of larger time steps ($\tau = 8h$), but in this case the higher order of convergence comes with a loss of positivity as also depicted in the bottom left picture of Figure 5.3. Concerning the mass conservation error, both new stabilized schemes show exponential convergence to zero in this example.

A visual comparison of our new stabilized schemes (with and without quadratic reconstruction) with the up-wind implicit and Gear's up-wind schemes is given in Figures 5.2, 5.3. In both Figures we only plot the numerical results for the S^{2}I^{2}OE scheme, as the results for the S^{1}I^{2}OE are the same as for S^{2}I^{2}OE in this example. The results in Figure 5.2 were obtained for $n = 1280$ and $\tau = 2h$, i.e. CFL$= 2$, while in Figure 5.3 $n = 1280$ and $\tau = 8h$, i.e. CFL$= 8$, were used. It can be observed that our new method is clearly superior to the classical implicit schemes in both cases. Although our new stabilized scheme is a little bit more diffusive when larger time steps are used, this effect is much more pronounced by the classical implicit up-wind scheme. In contrast, Gear's up-wind scheme does not preserve positivity and produces oscillations in the case of CFL$= 8$. A comparison of our new stabilized scheme with and without quadratic reconstruction shows that there is nearly no difference in the behavior of the scheme in this example. Thus, both variants may be used and produce nice results also for large time steps which exceed the CFL restriction.

5.2. 2D advection by a constant velocity vector field and by a rotation. First, let us consider a second order radially symmetric polynomial initial function in the form of paraboloid $u_0(x_1, x_2) = x_1^2 + x_2^2 - 0.25$ and the vector field $\mathbf{v}(x_1, x_2) = (-x_2, x_1)$ which rotates the initial function around the origin. Since it is radially symmetric the exact solution does not change in time. This test problem as well as all further 2D examples in this section are solved in the spatial domain $\Omega = (-1, 1) \times (-1, 1)$ which is split into $n \times n$ finite volumes. The time interval $(0, T)$ is equal $(0, 1)$ for this example and one can see in Table 5.4 that the exact solution is reproduced numerically up to machine precision by any of the I^{2}OE methods. The system matrix and the right hand side of the I^{2}OE method is constructed in such way that it does not touch this exact solution, which holds true in this case also for the stabilized methods.

The second example represents transport of the quadratic polynomial $u_0(x_1, x_2) = 2x_1^2 + x_2^2 - x_1 + x_2 - 0.25$ by the constant vector field $\mathbf{v}(x_1, x_2) = (-1.0, 0.5)$. We

Table 5.5

2D paraboloid transported by a constant vector field: report on the $L^1(I, L^1)$ errors of the I^{2}OE*,* S^{1}I^{2}OE*, and* S^{2}I^{2}OE *methods for refined space and time step sizes.*

			I^{2}OE	S^{1}I^{2}OE	S^{2}I^{2}OE
n	τ	NTS	$L^1(I, L^1)$	$L^1(I, L^1)$	$L^1(I, L^1)$
20	0.1	10	$2.624\ 10^{-15}$	$1.838\ 10^{-2}$	$5.544\ 10^{-3}$
40	0.05	20	$8.170\ 10^{-15}$	$2.959\ 10^{-3}$	$1.084\ 10^{-3}$
80	0.025	40	$1.421\ 10^{-14}$	$4.987\ 10^{-4}$	$2.315\ 10^{-4}$
160	0.0125	80	$2.045\ 10^{-14}$	$8.291\ 10^{-5}$	$4.537\ 10^{-5}$

Table 5.6

2D rotating paraboloid centered outside the origin: report on the $L^1(I, L^1)$ errors of the I^{2}OE*,* S^{1}I^{2}OE*, and* S^{2}I^{2}OE *methods for refined space and time step sizes.*

			I^{2}OE	S^{1}I^{2}OE	S^{2}I^{2}OE
n	τ	NTS	$L^1(I, L^1)$	$L^1(I, L^1)$	$L^1(I, L^1)$
20	0.157	20	$2.042\ 10^{-2}$	$3.184\ 10^{-2}$	$2.340\ 10^{-2}$
40	0.0785	40	$4.564\ 10^{-3}$	$6.422\ 10^{-3}$	$5.501\ 10^{-3}$
80	0.03925	80	$1.068\ 10^{-3}$	$1.379\ 10^{-3}$	$1.225\ 10^{-3}$
160	0.019625	160	$2.571\ 10^{-4}$	$3.104\ 10^{-4}$	$2.897\ 10^{-4}$

can see in Table 5.5 that, as given by the theory, the numerical solution by the I^{2}OE scheme is exact up to a machine precision, while the two stabilized methods are second order.

In the third example we consider the same paraboloid as in the first example but shifted to $(0.5, 0)$, i.e. $u_0(x_1, x_2) = (x_1 - 0.5)^2 + x_2^2 - 0.25$ and the same rotational vector field. The problem is solved in the larger time interval $(0, 3.14)$. All I^{2}OE methods are second order accurate, as one can see in Table 5.6. Here, no special attention to a CFL condition was given when choosing τ and h.

In the next two experiments we test the I^{2}OE methods in the case of standard 2D benchmarks, the rotations of a smooth hump and a discontinuous function around the origin, i.e. $\mathbf{v}(x_1, x_2) = (-x_2, x_1)$. The initial smooth function is given by $u_0(x_1, x_2) = \cos^5(\pi\sqrt{(x_1 + 0.5)^2 + x_2^2})$ inside a circle with radius 0.5 centered in $(-0.5, 0)$ and by 0 elsewhere. In the case of a rotating cylinder we have $u_0(x_1, x_2) = 1$ inside a circle with radius 0.45 centered in $(-0.5, 0)$ and 0 elsewhere. We compute the numerical solutions until for half a rotation ($T = 3.14$) without any special care to the CFL condition. In case of the smooth hump rotation we see second order convergence and very precise conservation of the rotating shape, cf. Table 5.7 and Figure 5.4. In case of the discontinuous solution we see a convergence rate of about $2/3$ for the stabilized I^{2}OE schemes and also good conservation of the initial shape after half a rotation, cf. Table 5.8 and Figure 5.5. This is much better than for any other standard implicit scheme with large time steps.

5.3. 2D advection by non-divergence free velocities including advective level set motion in normal direction with topological changes. In the next example we test the I^{2}OE schemes for transport in the non-divergence free velocity field

$$\mathbf{v}(x) = -\frac{x}{|x|}, x = (x_1, x_2). \tag{5.1}$$

Table 5.7

2D rotating smooth hump centered outside the origin: report on the $L^1(I, L^1)$ errors of the I^{2}OE, S^{1}I^{2}OE, *and* S^{2}I^{2}OE *methods for refined space and time step sizes.*

n	τ	NTS	I^{2}OE $L^1(I, L^1)$	S^{1}I^{2}OE $L^1(I, L^1)$	S^{2}I^{2}OE $L^1(I, L^1)$
20	0.157	20	$4.563\ 10^{-1}$	$2.680\ 10^{-1}$	$2.888\ 10^{-1}$
40	0.0785	40	$1.628\ 10^{-1}$	$1.210\ 10^{-1}$	$1.220\ 10^{-1}$
80	0.03925	80	$4.426\ 10^{-2}$	$3.927\ 10^{-2}$	$3.084\ 10^{-2}$
160	0.019625	160	$1.112\ 10^{-2}$	$1.091\ 10^{-2}$	$1.061\ 10^{-2}$
320	0.0098125	320	$2.767\ 10^{-3}$	$2.824\ 10^{-3}$	$2.772\ 10^{-3}$
640	0.00490625	640	$6.8982\ 10^{-4}$	$7.067\ 10^{-4}$	$6.993\ 10^{-4}$

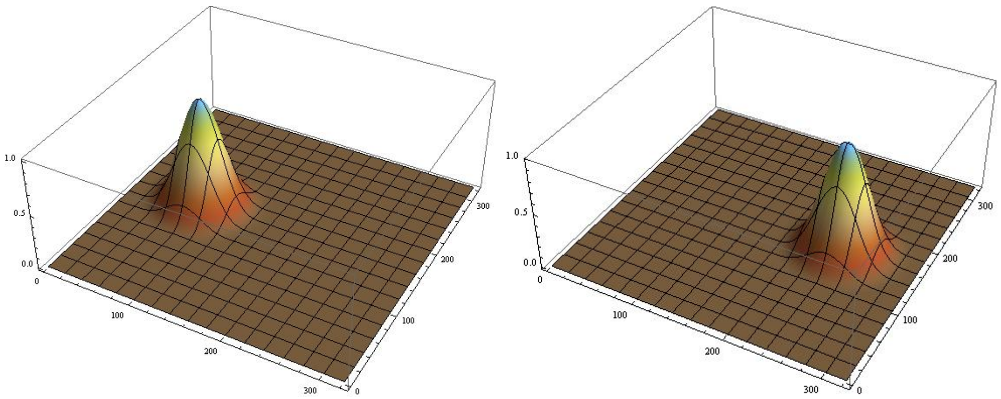

Fig. 5.4. *2D rotating smooth hump centered outside the origin: the initial condition (left) and the S^2I^2OE numerical solution after half a rotation (right), $n = 320$, cf. Table 5.7.*

The exact solution is given by $u(x, t) = u_0(x + \frac{tx}{|x|})$ where $u_0(x)$ is an initial profile. We consider the initial function $u_0(x_1, x_2) = -x_1^2 - x_2^2 + 1$ and solve the problem in the time interval $(0, 0.6)$ on subsequently refined grids. In this case there is a point singularity formed in the origin due to subsequent arrival of initial function values from circular neighborhoods. For this example all I^{2}OE methods are second order accurate and give similar results as one can see in Table 5.9.

In the last example of this section we look at level set motion in normal direction with topological changes. In detail we consider the resolution of the topological changes for the shrinking of an initial quatrefoil (top left in Figure 5.6) by a velocity field in normal direction with constant speed equal to 1. Thus, the vector field now depends on the solution and is given by $\mathbf{v} = -\frac{\nabla u}{|\nabla u|}$, cf. alsoSection 3.2. In the further plots of Figure 5.6 we present the evolution of the zero level line representing the quatrefoil evolution (left column) and 2D (middle column) and 3D (right column) plots of the evolution of the level set function u computed by the S^{2}I^{2}OE scheme, $n = 640$, $\tau = 2h$. For further numerical results of I^{2}OE schemes in the level set context we refer to [12] and the discussions therein.

Table 5.8

2D rotating cylinder centered outside the origin: report on the $L^1(I, L^1)$ errors of the $\mathrm{I^2OE}$, $\mathrm{S^1I^2OE}$, *and* $\mathrm{S^2I^2OE}$ *methods for successively refined space and time step sizes.*

			$\mathrm{I^2OE}$	$\mathrm{S^1I^2OE}$	$\mathrm{S^2I^2OE}$
n	τ	NTS	$L^1(I, L^1)$	$L^1(I, L^1)$	$L^1(I, L^1)$
20	0.157	20	$1.532\ 10^{0}$	$8.979\ 10^{-1}$	$9.004\ 10^{-1}$
40	0.0785	40	$1.161\ 10^{0}$	$5.758\ 10^{-1}$	$5.820\ 10^{-1}$
80	0.03925	80	$8.612\ 10^{-1}$	$3.698\ 10^{-1}$	$3.769\ 10^{-1}$
160	0.019625	160	$6.357\ 10^{-1}$	$2.374\ 10^{-1}$	$2.431\ 10^{-1}$
320	0.0098125	320	$4.668\ 10^{-1}$	$1.521\ 10^{-1}$	$1.560\ 10^{-1}$
640	0.00490625	640	$3.413\ 10^{-1}$	$9.720\ 10^{-2}$	$9.998\ 10^{-2}$

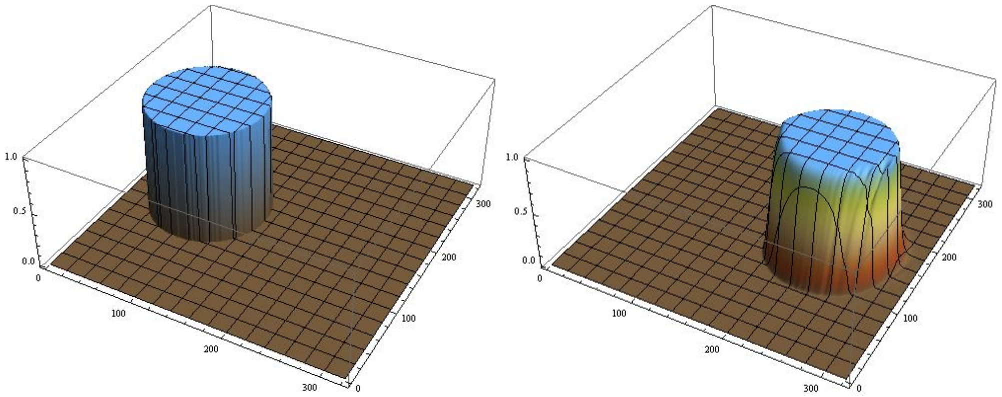

Fig. 5.5. *2D rotating cylinder centered outside the origin: the initial condition (left) and the S^2I^2OE numerical solution after half a rotation (right), $n = 320$, cf. Table 5.8.*

Table 5.9

Transport in the non-divergence free velocity field (5.1) *with singular solution in the origin: report on the $L^1(I, L^1)$ errors of the* $\mathrm{I^2OE}$, $\mathrm{S^1I^2OE}$, *and* $\mathrm{S^2I^2OE}$ *methods for successively refined space and time step sizes.*

			$\mathrm{I^2OE}$	$\mathrm{S^1I^2OE}$	$\mathrm{S^2I^2OE}$
n	τ	NTS	$L^1(I, L^1)$	$L^1(I, L^1)$	$L^1(I, L^1)$
20	0.1	6	$6.572\ 10^{-3}$	$6.572\ 10^{-3}$	$6.572\ 10^{-3}$
40	0.05	12	$1.480\ 10^{-3}$	$1.480\ 10^{-3}$	$1.480\ 10^{-3}$
80	0.025	24	$3.504\ 10^{-4}$	$3.504\ 10^{-4}$	$3.504\ 10^{-4}$
160	0.0125	48	$8.521\ 10^{-5}$	$8.521\ 10^{-5}$	$8.521\ 10^{-5}$
320	0.00625	96	$2.101\ 10^{-5}$	$2.101\ 10^{-5}$	$2.101\ 10^{-5}$

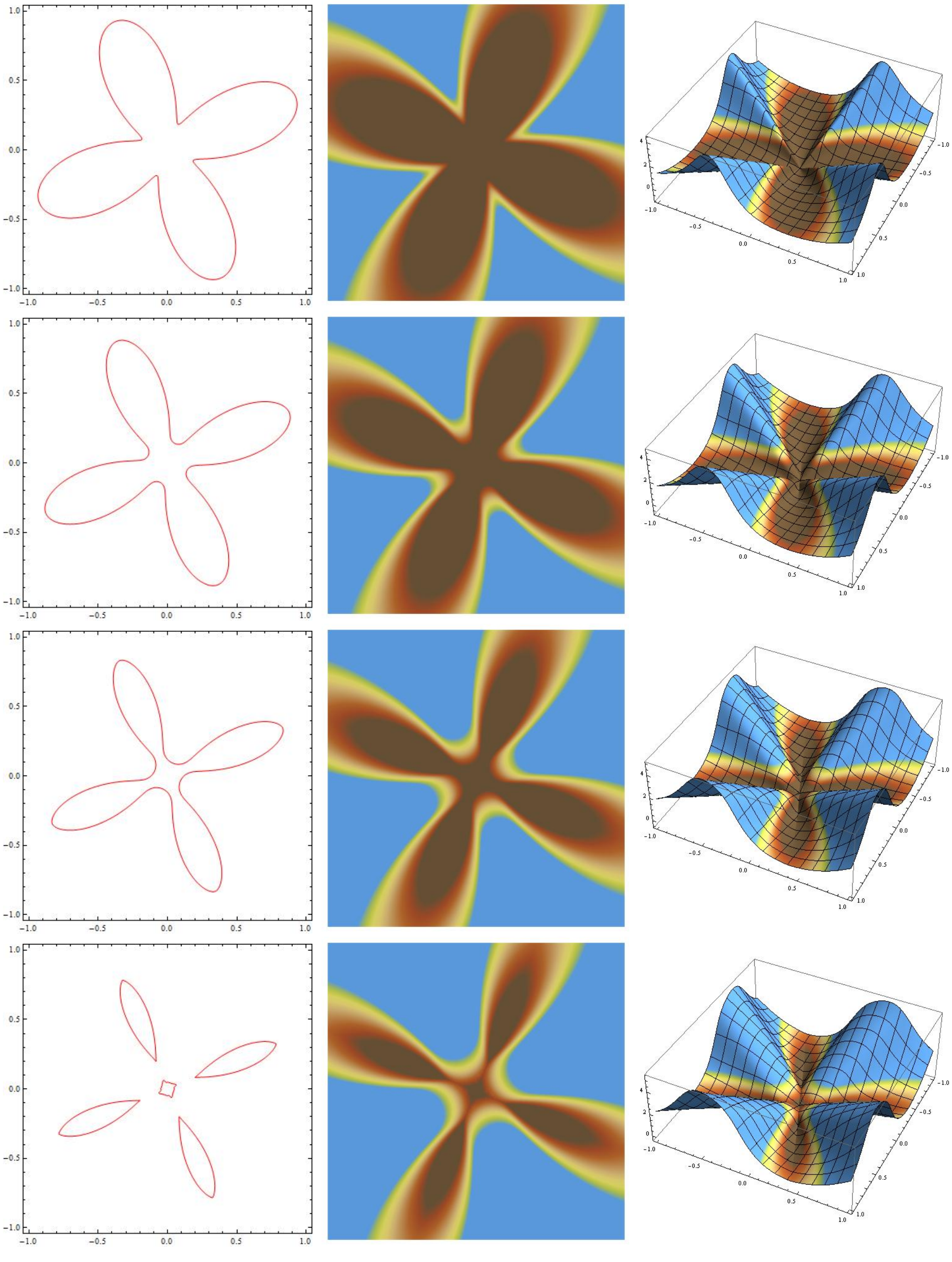

Fig. 5.6. *2D level set motion in normal direction: shrinking of the quatrefoil with topological changes. The numerical solution is plotted at the discrete times 0, 0.05, 0.1, 0.15. The zero level line representing the quatrefoil evolution is plotted in the left column, the 2D color coded level set function in the middle and a 3D visualization of the level set function in the right column.*

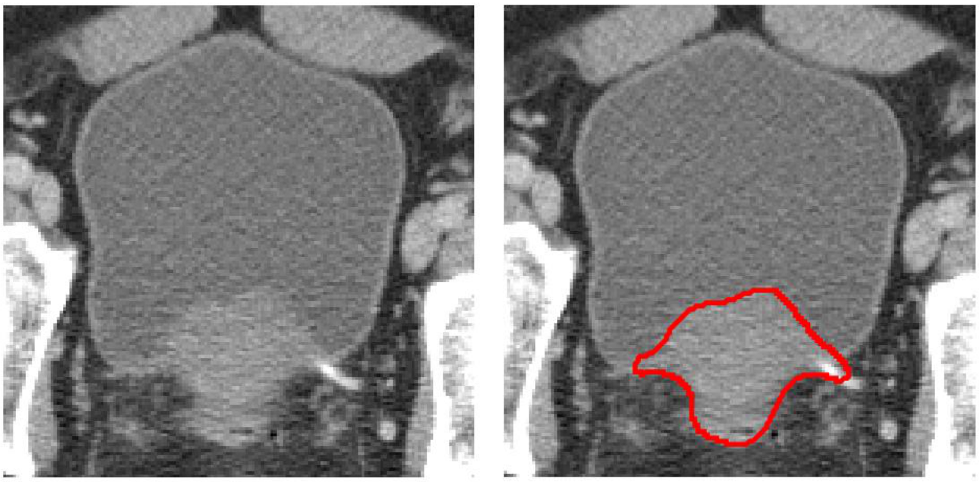

FIG. 5.7. *Prostate segmentation: 2D image (left) and the same image together with a red contour representing segmentation of the prostate by GSUBSURF model (5.2) using the S^2I^2OE scheme in the advective part.*

5.4. 2D medical image segmentation. In the last numerical experiment we present an application of the S^{2}I^{2}OE scheme in medical image segmentation. Here, we segment a 2D image with resolution 150 x 150 pixels, plotted in Figure 5.7 left, with the goal to precisely extract the prostate. Prostate segmentation is a very difficult task in medical image analysis due to a poor contrast and a high level of noise intrinsically linked to the image. We use the so-called generalized subjective surface (GSUBSURF) model which represents a robust method for biomedical image segmentation and is a useful generalization of the original approach presented in [17]. The GSUBSURF model has the form of the following PDE [15, 20, 3]

$$u_t - w_a \nabla g \cdot \nabla u - w_d g \sqrt{\varepsilon^2 + |\nabla u|^2} \nabla \cdot \left(\frac{\nabla u}{\sqrt{\varepsilon^2 + |\nabla u|}} \right) = 0, \tag{5.2}$$

where $u(t, x)$ is an evolving segmentation function starting from an initial condition, $u(0, x) = u_0(x)$, usually given by a peak located approximately in the center of the mass of the segmented object. Then, the segmentation function is evolved by the advection (the second term on the left hand side of (5.2)) regularized by the mean curvature flow (the third term on the left hand side of (5.2)) to a shock-like profile. The central isoline of this profile gives the segmentation result, for the segmentation function evolution see Figure 5.9 and for the resulting isoline, which gives very precise localization of the prostate see Figure 5.7, right. The important part of the model is given by the advection with the nontrivial velocity vector field $-w_a \nabla g$ where the function $g = \frac{1}{1+Ks^2}$ depends on the norm of the gradient $s = |\nabla I|$ of the image intensity function I smoothed by the mean curvature flow filter [6]. This nontrivial velocity field points towards the edges in the image. Its details in the prostate region are plotted in Figure 5.8. Opposite to previous implementations of the GSUBSURF model [15, 20, 3] where the advective part was treated by an explicit scheme – which put a severe restriction to the computational time step – we use here the S^{2}I^{2}OE scheme with a time step size exceeding more than 10 times the standard CFL condition. Similarly to [15, 3], for the curvature part we use an unconditionally stable

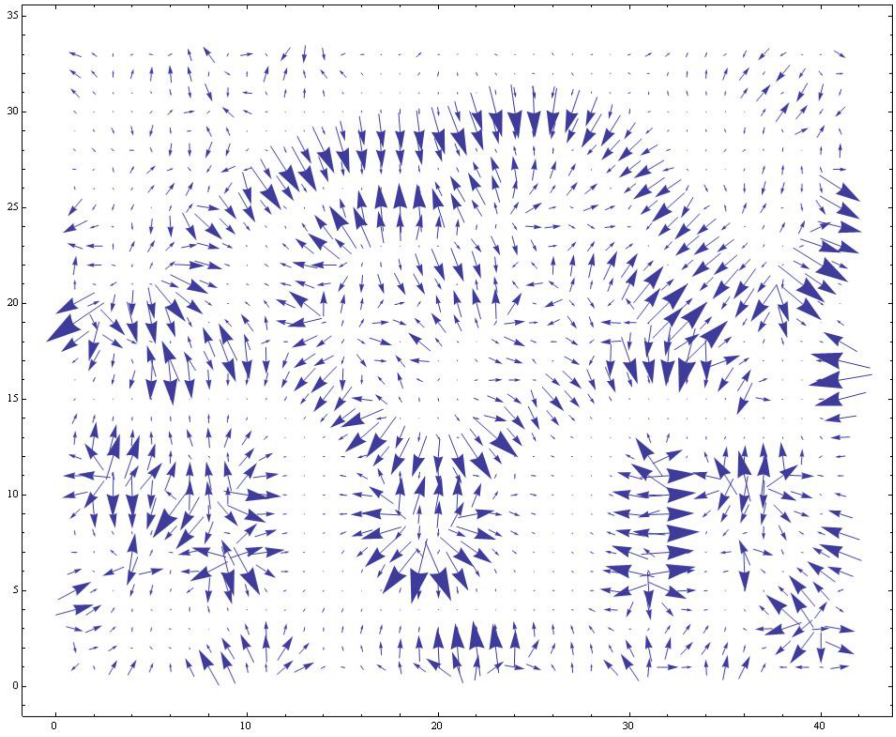

Fig. 5.8. *Prostate segmentation: a detail of the nontrivial velocity vector field used in segmentation of the prostate.*

semi-implicit diamond-cell finite volume method. As one can see in the right picture of Figure 5.7, we obtain precise results using such overall semi-implicit scheme (both in advection and curvature). Moreover, this scheme always guarantees solvability of the system and stability of the computation and thus represents an important improvement of the GSUBSURF segmentation method. Since we are interested in coming to an "equilibrium" segmentation shape, the choice of larger time step sizes is important from the CPU–time point of view. The model and computational parameters in this example were $h = 0.5$ (pixel size), $\tau = 5h$, $K = 10000$, $\varepsilon^2 = 10^{-6}$, $w_a = 5h$, $w_d = 4h$.

6. Conclusions. In this article we introduced new stabilized I^{2}OE schemes for solving variable velocity advection equations. We gave some theoretical and numerical background with respect to solvability, local mass conservation, accuracy and stability for the basic I^{2}OE scheme and its stabilized versions. As demonstrated in several numerical benchmark problems, in particular the S^{2}I^{2}OE scheme with quadratic reconstruction shows very nice resolution and stability properties. It preserves all solvability and accuracy properties of the basic I^{2}OE scheme for smooth solutions, while at the same time statisfying strong L^∞-stability, even in settings with discontinuous solutions. Moreover, all presented I^{2}OE schemes keep their accuracy and stability properties for arbitrary large time step sizes which makes this family of methods particular attractive for real applications as demonstrated here for 2D medical image segmentation.

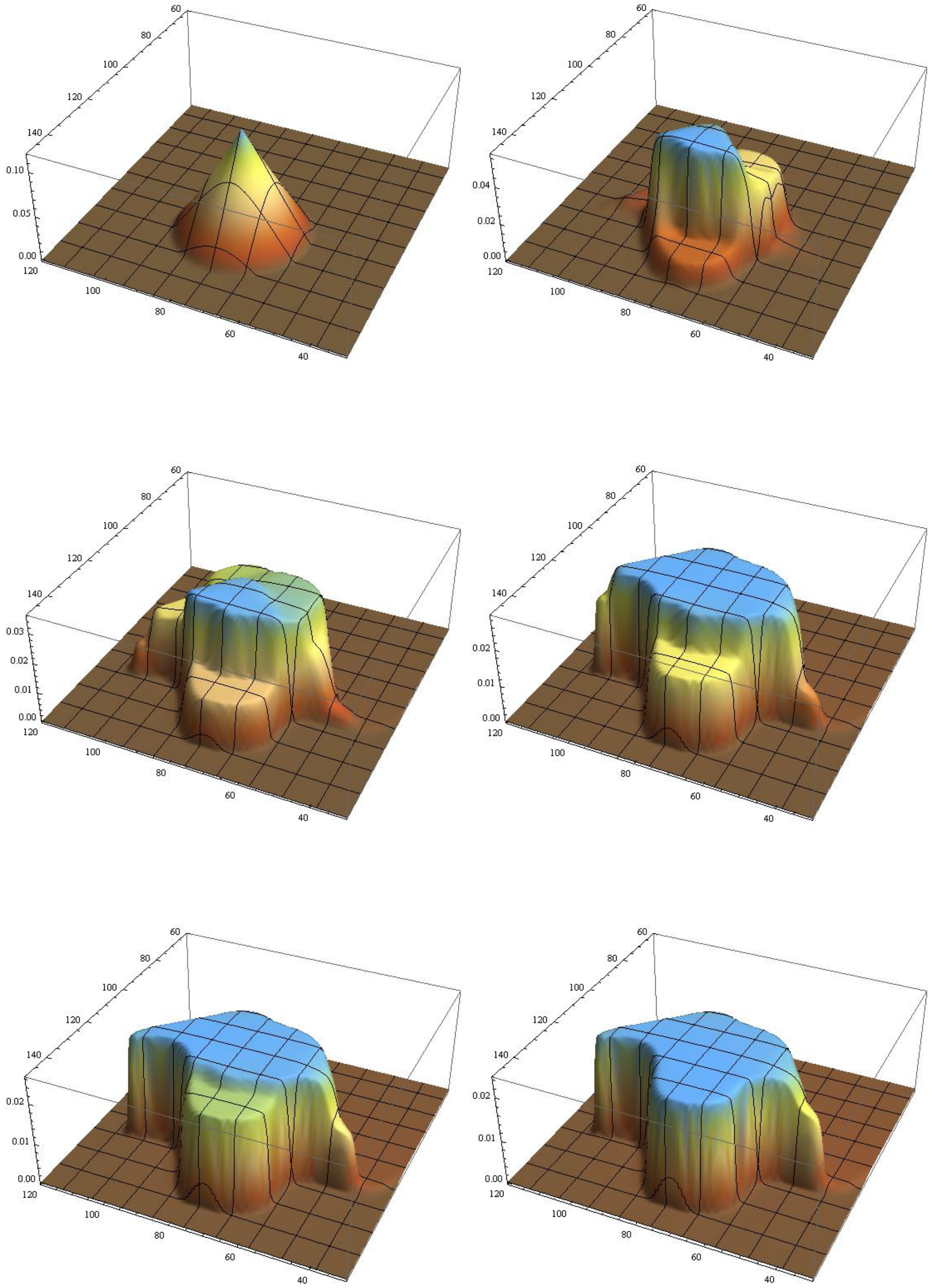

FIG. 5.9. *Prostate segmentation: graphs of subsequently evolving segmentation function, tending from the initial profile (top left) to the final shock-like shape (bottom right) which is used for extracting the segmentation contour plotted in red in Figure 5.7 right.*

7. Acknowledgment. The work of the first and third author was supported by the grants APVV-0184-10 and VEGA 1/0269/09.

REFERENCES

[1] M. Balažovjech, K. Mikula: A higher order scheme for a tangentially stabilized plane curve shortening flow with a driving force, SIAM Journal on Scientific Computing, Vol. 33, No. 5 (2011) pp. 2277-2294

[2] J.P. Boris, D.L. Book: Flux-corrected transport: I. SHASTA, a fluid transport algorithm that works, J. Comput. Phys., 11 (1973), pp. 38-69

[3] P. Bourgine, R. Čunderlík, O. Drblíková, K. Mikula, N. Peyriéras, M. Remešíková, B. Rizzi, A.S arti: 4D embryogenesis image analysis using PDE methods of image processing, Kybernetika, Vol. 46, No. 2 (2010).

[4] V. Caselles, R. Kimmel, G. Sapiro: Geodesic active contours. International Journal of Computer Vision, Vol. 22 (1997) pp. 61-79

[5] R. Eymard, T. Gallouet, R. Herbin: The finite volume methods, Handbook for Numerical Analysis, 2000, Vol. 7 (Ph. Ciarlet, J. L. Lions, eds.), Elsevier.

[6] R. Eymard, A. Handlovičová, K. Mikula: Study of a finite volume scheme for the regularised mean curvature flow level set equation, IMA Journal on Numerical Analysis, Vol. 31 (2011) pp. 813-846.

[7] P. Frolkovič, K. Mikula: Flux-based level set method: a finite volume method for evolving interfaces, Applied Numerical Mathematics, Vol. 57, No. 4 (2007) pp. 436-454.

[8] P. Frolkovič, K. Mikula: High-resolution flux-based level set method, SIAM Journal on Scientific Computing, Vol. 29, No. 2 (2007) pp. 579-597.

[9] S. Kichenassamy, A. Kumar, P. Olver, A. Tannenbaum, A. Yezzi: Conformal curva- ture flows: from phase transitions to active vision. Arch. Rational Mech. Anal. 134 (1996) pp. 275-301

[10] D. Kuzmin: Linearity-preserving flux correction and convergence acceleration for constrained Galerkin schemes, Journal of Computational and Applied Mathematics, 2011, http://dx.doi.org/10.1016/j.cam.2011.11.019

[11] R.J. LeVeque, Finite Volume Methods for Hyperbolic Problems, Cambridge Texts in Applied Mathematics. Cambridge University Press, 2002.

[12] K. Mikula, M. Ohlberger: A new level set method for motion in normal direction based on a semi-implicit forward-backward diffusion approach, SIAM J. Scientific Computing, Vol. 32, No. 3 (2010) pp. 1527-1544.

[13] K. Mikula, M. Ohlberger: Inflow-Implicit/Outflow-Explicit Scheme for Solving Advection Equations, in Finite Volumes in Complex Applications VI, Problems & Perspectives, Eds. J.Fořt et al. (Proceedings of the Sixth International Conference on Finite Volumes in Complex Applications, Prague, June 6-10, 2011), Springer Verlag, 2011, pp. 683-692.

[14] K. Mikula, M. Ohlberger: A new Inflow-Implicit/Outflow-Explicit Finite Volume Method for Solving Variable Velocity Advection Equations, Preprint 01/10 - N, Angewandte Mathematik und Informatik, Universitaet Münster, June 2010.

[15] K. Mikula, N. Peyrieras, M. Remešíková, A. Sarti: 3D embryogenesis image segmentation by the generalized subjective surface method using the finite volume technique, in Finite Volumes for Complex Applications V: Problems and Perspectives (Eds. R.Eymard, J.M.Herard), ISTE and WILEY, London, 2008, pp. 585-592.

[16] K. Mikula, D. Ševčovič, M. Balažovjech: A simple, fast and stabilized flowing finite volume method for solving general curve evolution equations, Communications in Computational Physics, Vol. 7, No. 1 (2010) pp. 195-211

[17] A. Sarti, R. Malladi, and J.A. Sethian: Subjective Surfaces: A Method for Completing Missing Boundaries, Proceedings of the National Academy of Sciences of the United States of America, vol. 12, pp. 6258-6263, 2000

[18] J.A. Sethian: Level Set Methods and Fast Marching Methods: Evolving Interfaces in Computational Geometry, Fluid Mechanics, Computer Vision, and Material Science, Cambridge University Press, New York, 1999.

[19] S.T. Zalesak: Fully multidimensional flux-corrected transport algorithms for fluids, J. Comput. Phys., Vol. 31 (1979) pp.335-362

[20] C. Zanella, M. Campana, B. Rizzi, C. Melani, G. Sanguinetti, P. Bourgine, K. Mikula, N. Peyrieras, A. Sarti: Cells Segmentation from 3-D Confocal Images of Early Zebrafish Embryogenesis, IEEE Transactions on Image Processing, Vol.19, No.3 (2010) pp. 770-781

Preprints
”Angewandte Mathematik und Informatik”

02/09 - N P. Henning, M. Ohlberger: Advection-diffusion problems with rapidly oscillating coefficients and large expected drift. Part 1: Homogenization – existence, uniqueness and regularity

03/09 - N P. Henning, M. Ohlberger: Advection-diffusion problems with rapidly oscillating coefficients and large expected drift. Part 2: The heterogeneous multiscale finite element method

04/09 - I J. Meyer-Spradow, T. Ropinski, J. Mensmann, K. Hinrichs: Rapid Prototyping of Volume Visualization in Collaboration with Domain Experts

05/09 - N K. Mikula, M. Ohlberger: A New Level Set Methof for Motion in Normal Direction Based on a Forward-Backward Diffusion Formulation

06/09 - I T. Ropinski, S. Diepenbrock, S. Bruckner, K. Hinrichs, E. Gröller: Volumetric Texturing

07/09 - I J.-S. Praßni, J. Mensmann, T. Ropinski, K. Hinrichs: Shape-based Transfer Functions for Volume Visualization

08/09 - N A. Dedner, R. Klöfkorn, M. Nolte, M. Ohlberger: A generic interface for parallel and adaptive scientific computing: Abstraction principles and the DUNE-FEM module

09/09 - N P. Henning, M. Ohlberger: A-posteriori error estimate for a heterogeneous multiscale finite element method for advection-diffusion problems with rapidly oscillating coefficients and large expected drift

01/10 - N K. Mikula, M. Ohlberger: A New Inflow-Implicit/Outflow-Explicit Finie Volume Method for Solving Variable Velocity Advection Equations

02/10 - N M. Drohmann, B. Haasdonk, M. Ohlberger: Reduced Basis Approximation for Nonlinear Parametrized Evolution Equations based on Empirical Operator Interpolation

03/10 - N M. Ohlberger, K. Smetana: A new problem adapted hierarchical model reduction technique based on reduced basis methods and dimensional splitting

04/10 - I M. Steuwer, P. Kegel, S. Gorlatch: SkelCL – A Portable Multi-GPU Skeleton Library

01/11 - N P. Henning, M. Ohlberger: A-posteriori error estimation for a heterogeneous multiscale method for monotone operators and beyond a periodic setting

02/11 - N M. Ohlberger, K. Smetana: A new Hierarchical Model Reduction-Reduced Basis technique for advection-diffusion-reaction problems

03/11 - N S. Kaulmann, M. Ohlberger, B. Haasdonk: A New Local Reduced Basis Discontinuous Galerkin Approach for Heterogeneous Multiscale Problems

04/11 - N P. Henning: Convergence of MsFEM approximations for elliptic, non-periodic homogenization problems

01/12 - N K. Mikula, M. Ohlberger, J. Urbán: Inflow-Implicit/Outflow-Explicit Finite Volume Methods for Solving Advection Equations